Inorganic Chemistry

Article

pubs.acs.org/IC

Photoinduced Electron and Energy Transfer and pH-Induced Modulation of the Photophysical Properties in Homo- and Heterobimetallic Complexes of Ruthenium(II) and Rhodium(III) Based on a Heteroditopic Phenanthroline–Terpyridine Bridge

Dinesh Maity, Chanchal Bhaumik, Srikanta Karmakar, and Sujoy Baitalik*

Inorganic Chemistry Section, Department of Chemistry, Jadavpur University, Kolkata 700032, India

Supporting Information

ABSTRACT: Homo- and heterobimetallic complexes of compositions $[(bpy)_2Ru^{II}(phen\text{-}Hbzim\text{-}tpy)Ru^{II}(tpy/tpy\text{-}PhCH_3/H_2pbbzim)]^{4+}$ and $[(bpy)_2Ru^{II}(phen\text{-}Hbzim\text{-}tpy)\text{-}Rh^{III}(tpy\text{-}PhCH_3/H_2pbbzim)]^{5+}$, where phen-Hbzim-tpy = 2-[4-(2,6-dipyridin-2-ylpyridin-4-yl)phenyl]-1*H*-imidazole[4,5-*f*][1,10]phenanthroline, bpy = 2,2′-bipyridine, tpy = 2,2′:6′,2″-terpyridine, tpy-$PhCH_3$ = 4′-(4-methylphenyl)-2,2′:6′,2″-terpyridine, and H_2pbbzim = 2,6-bis(benzimidazol-2-yl)-pyridine, have been synthesized and characterized by elemental analyses, electrospray ionization mass spectrometry, and ^{1}H NMR spectroscopy. The absorption spectra, redox behavior, and luminescence properties of these bimetallic complexes have been thoroughly investigated and compared with those of monometallic $[(bpy)_2Ru^{II}(phen\text{-}Hbzim\text{-}tpy)]^{2+}$ and $[(tpy\text{-}PhCH_3)Rh^{III}(tpy\text{-}Hbzim\text{-}phen)]^{3+}$ model compounds. The electrochemistry of the complexes shows a reversible $Ru^{II/III}$ oxidation in the anodic region and an irreversible $Rh^{III/I}$ reduction and several ligand-based reductions in the cathodic region. Steady-state and time-resolved luminescence data at room temperature show that an efficient intramolecular electronic energy transfer from the metal-to-ligand charge-transfer (MLCT) excited state of the $[(bpy)_2Ru^{II}(phen\text{-}Hbzim\text{-}tpy)]$ chromophore to the MLCT state of the tpy-containing chromophore $[(phen\text{-}Hbzim\text{-}tpy)Ru^{II}(tpy/tpy\text{-}PhCH_3/H_2pbbzim)]$ occurs in all three unsymmetrical homobimetallic complexes. On the other hand, for both heterometallic dyads, an efficient intramolecular photoinduced electron transfer from the excited ruthenium moiety to the rhodium-based unit takes place. The rate constants for the energy- and electron-transfer processes have been determined by time-resolved emission spectroscopy. The influence of the pH on the absorption, steady-state, and time-resolved emission properties of complexes has been thoroughly investigated. The absorption titration data were used to determine the ground-state p*K* values, whereas the luminescence data were utilized for determination of the excited-state acid dissociation constants. In effect, deprotonation of the azole NH moieties of the complexes leads to a substantial lowering of the MLCT absorption and emission band energies.

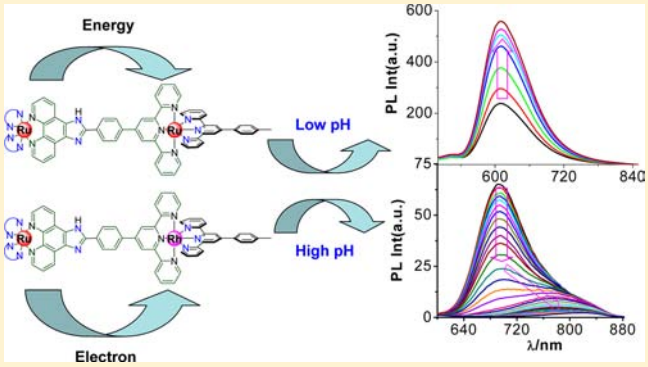

INTRODUCTION

Intramolecular electron- and energy-transfer processes in di- and oligonuclear d^6 transition-metal polypyridine complexes whose mononuclear entities are linked by conjugated bridging ligands have received considerable attention because cooperative interactions between metal centers in these complexes give rise to properties that are useful for constructing photomolecular devices.[1−3] The directional flow of electron and/or energy gets facilitated when there is asymmetry in the multicomponent system. Such asymmetry can be introduced by either using ligands that differ in donor−acceptor properties or using heterometallic sites. The features associated with bridging ligands such as length, rigidity, topology, conjugation, charge, and numbers of dissociable hydrogen atoms play important roles in this context.[1−3] Two types of polypyridine bridging ligands are generally used for this study. The first type, which has found maximum use, contains bidentate chelating sites like 2,2′-bipyridine (bpy) or 1,10-phenanthroline (phen), either directly coupled or linked by a spacer.[1] The second type of ligand, on the other hand, contains tridentate chelating sites such as 2,2′:6′,2″-terpyridine (tpy).[1,4] A large number of mono-, bi-, and multimetallic complexes are now known, notably built around bpy, phen, or tpy ligands, and have been used for various applications.[1−7] The choice of the bridging ligands based on bpy-type chelating sites is appropriate from electronic and photophysical viewpoints. In terms of structure, however, such a choice is not ideal because substitution of a single position in a bpy ligand will lead to the formation of diastereomeric products. The tridentate tpy-type ligand is more

Received: February 20, 2013
Published: June 25, 2013

   dx.doi.org/10.1021/ic400449c | *Inorg. Chem.* 2013, 52, 7933−7946

Chart 1

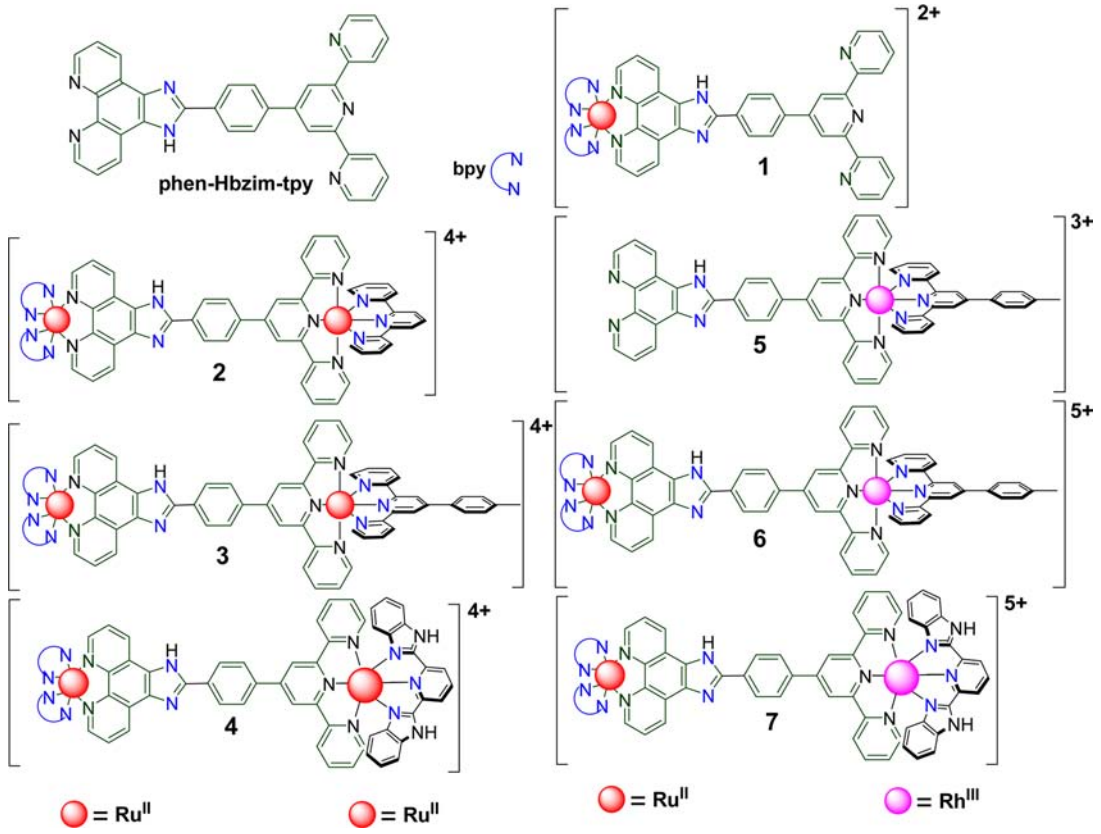

appealing from the viewpoint of constructing linear, rodlike polynuclear complexes.[4] However, usually such complexes are practically nonluminescent at room temperature and their excited-state lifetimes (τ = 0.25 ns for $[Ru(tpy)_2]^{2+}$)[1a] are also very short and therefore are the major deterrents for them to act as photosensitizers. Consequently, much effort has been devoted to designing and synthesizing tridentate polypyridine ligands that can produce ruthenium(II) complexes with enhanced emission quantum yields and excited-state lifetimes.[4] Compared to the tris-bidentate and bis-terdentate complexes, rigidly linked homo- and heterometallic assemblies comprising a combination of bis-terdentate and tris-bidentate complexes are extremely rare, despite the very interesting properties that could be expected from the unique attributes of each type of complex.[8−11]

Recently, we reported the synthesis, structural characterization, and photophysical and anion-sensing properties of several terpyridylimidazole ligands and their ruthenium(II) and osmium(II) complexes.[12] In our search for the appropriate bpy-tpy- or phen-tpy-type bridging ligand, we have found the 2-[4-(2,6-dipyridin-2-ylpyridin-4-yl)phenyl]-1*H*-imidazole[4,5-*f*]-[1,10]phenanthroline (phen-Hbzim-tpy) system, which has yet to be exploited in the area for the construction of rigidly linked homo- and heterometallic complexes comprising a combination of bis-terdentate and tris-bidentate moieties (Chart 1). During the course of our investigation, Hamelin and co-workers synthesized a Ru-bpy-based dyad containing the same ligand phen-Hbzim-tpy and showed that the complex upon photoexcitation is able to catalyze selective sulfide oxygenation involving an oxygen atom transfer from water to the substrate.[13] In this contribution, we will demonstrate the formation of unprecedented bimetallic systems comprising one metal center (Ru^{II}) coordinated by three bidentate ligands (bpy or phen) and a second metal center (Ru^{II} or Rh^{III}) coordinated by two tridentate (tpy/tpy-$PhCH_3$/H_2pbbzim) ligands. Selective incorporation of a Rh^{III} unit in this way is expected to be difficult owing to the very robust conditions required for coordination. However, such units are highly attractive as energy donors because of their high excited-state energies. Moreover, all of the complexes have dissociable imidazole NH proton(s). We will be interested in studying pH-induced switching of the photophysical properties of these complexes because the design and synthesis of complexes that reversibly interchange between different forms prompted by external stimuli are currently of great interest in both fundamental and applied research.[14−16] The pH (protonation/deprotonation) can be used as an external stimulus for rapid switching of the molecular properties toward the development of promising functional molecules.[17,18] Indeed, depending upon the extent of perturbation of these properties, proton-driven molecular switches can be developed.[14−18] The present study is concerned with the synthesis, structural characterization, redox activities, and pH-induced modulation of the photophysical properties of three new homodimetallic ruthenium(II)−ruthenium(II) and two heterodimetallic ruthenium(II)−rhodium(III) complexes based on the use of heteroditopic phen-Hbzim-tpy as a bridging ligand. As will be seen, significant changes in the absorbances and steady-state and time-resolved luminescence properties of such complexes can be brought about by changing the pH of the solution.

EXPERIMENTAL SECTION

Materials. Reagent-grade chemicals obtained from commercial sources were used as received. Solvents were purified and dried

dx.doi.org/10.1021/ic400449c | *Inorg. Chem.* 2013, 52, 7933−7946

according to standard methods. 1,10-Phenanthroline (phen), 2,2′:6′,2″-terpyridine (tpy), 2,6-pyridinedicarboxylic acid, and 1,2-phenylenediamine were purchased from Sigma-Aldrich. 1,10-Phenanthroline-5,6-dione,[19] 4′-(*p*-methylphenyl)-2,2′:6′,2″-terpyridine (tpy-PhCH$_3$),[12e,20] 4′-(*p*-formylphenyl)-2,2′:6′,2″-terpyridine (tpy-PhCHO),[21] 2,6-bis(benzimidazol-2-yl)pyridine (H_2pbbzim),[22] the bridging 2-[4-(2,6-dipyridin-2-ylpyridine-4-yl)phenyl]-1*H*-imidazole-[4,5-*f*][1,10]phenanthroline (phen-Hbzim-tpy) ligand,[13] and *cis*-[Ru(bpy)$_2$Cl$_2$]·2H$_2$O[23] were synthesized according to literature procedures. AgClO$_4$ was prepared from silver carbonate and perchloric acid and recrystallized from benzene. [(tpy-PhCH$_3$)RuCl$_3$] and [(H_2pbbzim)RuCl$_3$] were prepared by the reaction of RuCl$_3$·3H$_2$O with tpy-PhCH$_3$ and H_2pbbzim in a 1:1 molar ratio in refluxing ethanol. Again, [(tpy-PhCH$_3$)RhCl$_3$] and [(H_2pbbzim)RhCl$_3$] were prepared by the reaction of RhCl$_3$·3H$_2$O with tpy-PhCH$_3$ and H_2pbbzim in a 1:1 molar ratio in refluxing ethanol. The monometallic ruthenium(II) complex of composition [(bpy)$_2$Ru(phen-Hbzim-tpy)](ClO$_4$)$_2$ was prepared by a slight modification of a previously published literature procedure.[13]

Preparation of the Ligand phen-Hbzim-tpy. tpy-PhCHO (337 mg, 1.00 mmol), 1,10-phenanthroline-5,6-dione (230 mg, 1.10 mmol), and ammonium acetate (1.6 g, 20 mmol) were stirred in acetic acid (30 mL), and the mixture was refluxed for 2 h with continuous stirring. Upon cooling to room temperature, a pale-yellow crystalline compound deposited. The resulting compound was collected by filtration, washed several times with water, and then air-dried. The compound was finally recrystallized from a chloroform−methanol (1:1, v/v) mixture, and the desired compound was obtained as a light-yellow crystalline solid (340 mg, 0.64 mmol, yield 65%). ^{1}H NMR (300 MHz, DMSO-d_6, δ/ppm): 13.93 (s, 1H, NH imidazole), 9.04 (s, 2H, H3′), 8.95 (d, 2H, J = 7.5 Hz, H6), 8.82−8.75 (m, 2H, H9), 8.68 (d, 2H, J = 7.8 Hz, H3), 8.49 (d, 2H, J = 6.6 Hz, H8), 8.22 (d, 2H, J = 7.8 Hz, H7), 8.04 (t, 2H, J = 7.6 Hz, H4), 7.84 (br, 4H, 2H10 + 2H11), 7.54 (t, 2H, J = 5.8 Hz, H5). ESI-MS: m/z 528.22 ([L + H]$^+$). Anal. Calcd for C$_{34}$H$_{21}$N$_7$: C, 77.40; H, 4.01; N, 18.58. Found: C, 77.38; H, 4.03; N, 18.55.

Synthesis of the Metal Complexes. The complexes were prepared under oxygen and moisture-free dinitrogen using standard Schlenk techniques.

[(bpy)$_2$Ru(phen-Hbzim-tpy)](ClO$_4$)$_2$·4H$_2$O (**1**). To a stirred suspension of *cis*-[Ru(bpy)$_2$Cl$_2$]·2H$_2$O (0.52 g, 1 mmol) in ethanol (50 mL) was added solid AgClO$_4$ (0.43 g, 2.1 mmol). After 0.5 h, the precipitated AgCl was removed by quick filtration, and to the filtrate containing [Ru(bpy)$_2$(EtOH)$_2$]$^{2+}$ was added solid phen-Hbzim-tpy (0.64 g, 1.2 mmol). The resulting mixture was then refluxed for 5 h, during which time the color changed from blood red to reddish-yellow. Upon cooling to room temperature, a red precipitate was obtained, filtered, and dried under vacuum. The compound was then purified by recrystallization from an acetonitrile−methanol (1:1, v/v) mixture in the presence of a few drops of aqueous 10^{-4} M perchloric acid (1.03 g, yield 85%). Anal. Calcd for C$_{54}$H$_{45}$N$_{11}$Cl$_2$O$_{12}$Ru: C, 53.52; H, 3.74; N, 12.71. Found: C, 53.50; H, 3.72; N, 12.69. ^{1}H NMR [300 MHz, DMSO-d_6, δ/ ppm; see Scheme S1 (Supporting Information) for proton numbering]: 14.59 (s, 1H, NH imidazole), 9.17 (d, 2H, J = 8.1 Hz, H3″), 8.90−8.79 (m, 8H, 2H3″ + 2H3′ + 2H6 + 2H9), 8.71 (d, 2H, J = 7.8 Hz, H3), 8.56 (d, 2H, J = 8.2 Hz, H8), 8.30 (d, 2H, J = 8.3 Hz, H7), 8.22 (t, 2H, J = 7.7 Hz, H4), 8.14−8.04 (m, 6H, 2H4′ + 2H10 + 2H11), 7.95 (br, 2H, H4′), 7.85 (d, 2H, J = 5.3 Hz, H6′), 7.62−7.55 (m, 6H, 2H5′ + 2H6′ + 2H5), 7.36 (t, 2H, J = 6.5 Hz, H5′). UV−vis [CH$_3$CN; λ_{max}/nm (ε/M^{-1} cm^{-1})]: 460 (19750), 426 (sh, 15330), 326 (br, 51330), 288 (112250).

[(bpy)$_2$Ru(phen-Hbzim-tpy)Ru(tpy)](ClO$_4$)$_4$·2H$_2$O (**2**). A mixture of [Ru(tpy)Cl$_3$] (62 mg, 0.14 mmol), AgBF$_4$ (92 mg, 0.47 mmol), and 30 mL of acetone were refluxed with continuous stirring for 4 h. After the solution cooled to room temperature, the precipitated AgCl was removed by filtration. A total of 40 mL of EtOH was then added to the filtrate. Acetone was removed by rotary evaporation. To the resulting solution was added an ethanol solution of complex **1**, and the solution was refluxed for 6 h. Upon cooling, the deep-red compound that deposited was filtered and then dried under vacuum. The compound was redissolved in a minimum volume of acetonitrile and then subjected to silica gel column chromatography (eluent: acetonitrile). The eluent was rotary evaporated to a small volume (∼5 mL), and anion-exchange reaction with NaClO$_4$ gave rise to the desired compound. The compound was finally recrystallized from an acetonitrile−methanol (1:1, v/v) mixture in the presence of a few drops of aqueous 10^{-4} M perchloric acid (145 mg, yield 60%). Anal. Calcd for C$_{69}$H$_{52}$N$_{14}$Cl$_4$O$_{18}$Ru$_2$: C, 48.49; H, 3.07; N, 11.47. Found: C, 48.47; H, 3.09; N, 11.49. ^{1}H NMR (300 MHz, DMSO-d_6, δ/ppm): 14.63 (s, 1H, NH imidazole), 9.57 (s, 2H, H3′), 9.19−9.11 (m, 6H, 2H3′ + 4H6), 8.91−8.85 (m, 6H, 4H3″ + 2H9), 8.75−8.67 (m, 4H, 2H7 + 2H8), 8.56 (t, 1H, J = 8.0 Hz, H4″), 8.24 (t, 2H, J = 7.8 Hz, H4), 8.16−7.98 (m, 8H, 2H4 + 4H4′ + 2H6′), 7.87 (d, 2H, J = 5.3 Hz, H6′), 7.63−7.55 (m, 4H, 2H5′ + 2H11), 7.48 (d, 2H, J = 5.3 Hz, H10), 7.38 (t, 2H, J = 6.5 Hz, H5′), 7.33−7.22 (m, 6H, 4H3 + 2H5), 7.15 (t, 2H, J = 6.3, H5). ESI-MS (positive, CH$_3$CN) m/z 318.89 (100%) [(bpy)$_2$Ru(phen-Hbzim-tpy)Ru(tpy)]$^{4+}$, 424.89 (22%) [(bpy)$_2$Ru(phen-bzim-tpy)Ru(tpy)]$^{3+}$. UV−vis [CH$_3$CN; λ_{max}/nm (ε/M^{-1} cm^{-1})]: 486 (35660), 460 (sh, 32250), 365 (br, 35750), 332 (sh, 49660), 308 (sh, 71410), 286 (100750).

[(bpy)$_2$Ru(phen-Hbzim-tpy)Ru(tpy-PhCH$_3$)](ClO$_4$)$_4$·2H$_2$O (**3**). This compound was prepared in the same way as **2** using [(tpy-PhCH$_3$)RuCl$_3$] as the starting material. Yield: 65%. Anal. Calcd for C$_{76}$H$_{58}$N$_{14}$Cl$_4$O$_{18}$Ru$_2$: C, 50.73; H, 3.25; N, 10.90. Found: C, 50.71; H, 3.28; N, 10.92. ^{1}H NMR (500 MHz, DMSO-d_6, δ/ppm): 14.72 (s, 1H, NH imidazole), 9.54 (s, 2H, H3′), 9.43 (s, 2H, H3′), 9.19 (d, 2H, J = 7.5 Hz, H6), 9.09 (m, 4H, 2H6 + 2H9), 8.86 (d, 2H, J = 7.5 Hz, H3″), 8.83 (d, 2H, J = 8.0 Hz, H3″), 8.70 (nr, 4H, 2H7 + 2H8), 8.34 (nr, 2H, H8), 8.22 (t, 2H, J = 7.5 Hz, H4), 8.12−8.05 (m, 8H, 4H4′ + 2H6′ + 2H4), 7.98 (br, 2H, H6′), 7.87 (d, 2H, J = 5.0 Hz, H11), 7.64 (nr, 2H, H10), 7.57−7.55 (m, 6H, 4H3 + 2H7), 7.36 (t, 4H, J = 6.5 Hz, H5′), 7.29−7.27 (m, 4H, H5), 2.50 (s, 3H, CH$_3$). ESI-MS (positive, CH$_3$CN): m/z 341.26 (100%) [(bpy)$_2$Ru(phen-Hbzim-tpy)Ru(tpy-PhCH$_3$)]$^{4+}$, 454.70 (18%) [(bpy)$_2$Ru(phen-bzim-tpy)Ru-(tpy-PhCH$_3$)]$^{3+}$. UV−vis [CH$_3$CN; λ_{max}/nm (ε/M^{-1} cm^{-1})]: 492 (45160), 458 (br, 34580), 364 (br, 33830), 331 (br, 66160), 310 (sh, 99080), 286 (141160).

[(bpy)$_2$Ru(phen-Hbzim-tpy)Ru(H_2pbbzim)](ClO$_4$)$_4$·2H$_2$O (**4**). [(H_2pbbzim)RuCl$_3$] (73 mg, 0.14 mmol) was suspended in ethylene glycol (30 mL) and heated at 100 °C with continuous stirring. To the suspension was added **1** (180 mg, 0.15 mmol), and the reaction mixture was again heated at 180 °C for 12 h. The resulting solution was cooled, and the perchlorate salt of the complex was precipitated by pouring the solution into an aqueous solution of NaClO$_4$·H$_2$O (1.0 g in 10 mL of water). The precipitate obtained was filtered, washed with water, and dried under vacuum. The compound was then purified by silica gel column chromatography using a mixture of CH$_3$CN and 10% aqueous KNO$_3$ (10:1, v/v) as the eluent. Subsequent anion-exchange reaction with NaClO$_4$·H$_2$O gave rise to the desired compound. The compound was finally recrystallized from an acetonitrile−methanol (1:1, v/v) mixture in the presence of a few drops of aqueous 10^{-4} M perchloric acid (168 mg, yield 63%). Anal. Calcd for C$_{73}$H$_{54}$N$_{16}$Cl$_4$O$_{18}$Ru$_2$: C, 49.06; H, 3.04; N, 12.54. Found: C, 49.04; H, 3.06; N, 12.56. ^{1}H NMR (300 MHz, DMSO-d_6, δ/ppm): 15.05 (s, 2H, NH imidazole), 14.67 (s, 1H, NH imidazole), 9.67 (s, 2H, H3′), 9.20 (d, 2H, J = 7.6 Hz, H6), 9.04 (d, 2H, J = 8.1 Hz, H9), 8.91−8.85 (m, 6H, 2H7 + 2H8 + 2H11′), 8.79−8.71 (m, 4H, H3″), 8.63 (t, 1H, J = 7.9 Hz, H10′), 8.24 (t, 2H, J = 7.8 Hz, H4), 8.16−8.11 (m, 4H, 2H4′ + 2H11), 8.00−7.95 (m, 4H, 2H4′ + 2H10), 7.87 (d, 2H, J = 5.3 Hz, H6′), 7.68−7.59 (m, 8H, 2H3 + 4H5′ + 2H6′), 7.52 (d, 2H, J = 5.4 Hz, H12), 7.38 (t, 2H, J = 6.5 Hz, H5), 7.27 (t, 2H, J = 6.4 Hz, H13), 7.00 (t, 2H, J = 7.4 Hz, H14), 6.07 (d, 2H, J = 8.1 Hz, H15). ESI-MS (positive, CH$_3$CN): m/z 338.32 (100%) [(bpy)$_2$Ru(phen-Hbzim-tpy)Ru(H_2pbbzim)]$^{4+}$, 450.79 (78%) [(bpy)$_2$Ru(phen-Hbzim-tpy)-Ru(Hpbbzim)]$^{3+}$, 675.71 (10%) [(bpy)$_2$Ru(phen-Hbzim-tpy)Ru-(pbbzim)]$^{2+}$. UV−vis [CH$_3$CN; λ_{max}/nm (ε/M^{-1} cm^{-1})]: 480 (33660), 425 (sh, 22580), 373 (br, 44000), 348 (sh, 79830), 334 (sh, 76750), 315 (sh, 78500), 286 (128160).

[(tpy-PhCH$_3$)Rh(tpy-Hbzim-phen)](BF$_4$)$_3$·3H$_2$O (**5**). A solution of [(tpy-PhCH$_3$)Rh(acetone)$_3$]$^{3+}$ was prepared by stirring a mixture of

dx.doi.org/10.1021/ic400449c | Inorg. Chem. 2013, 52, 7933−7946

Scheme 1. Synthesis of Homo- and Heterometallic Complexes

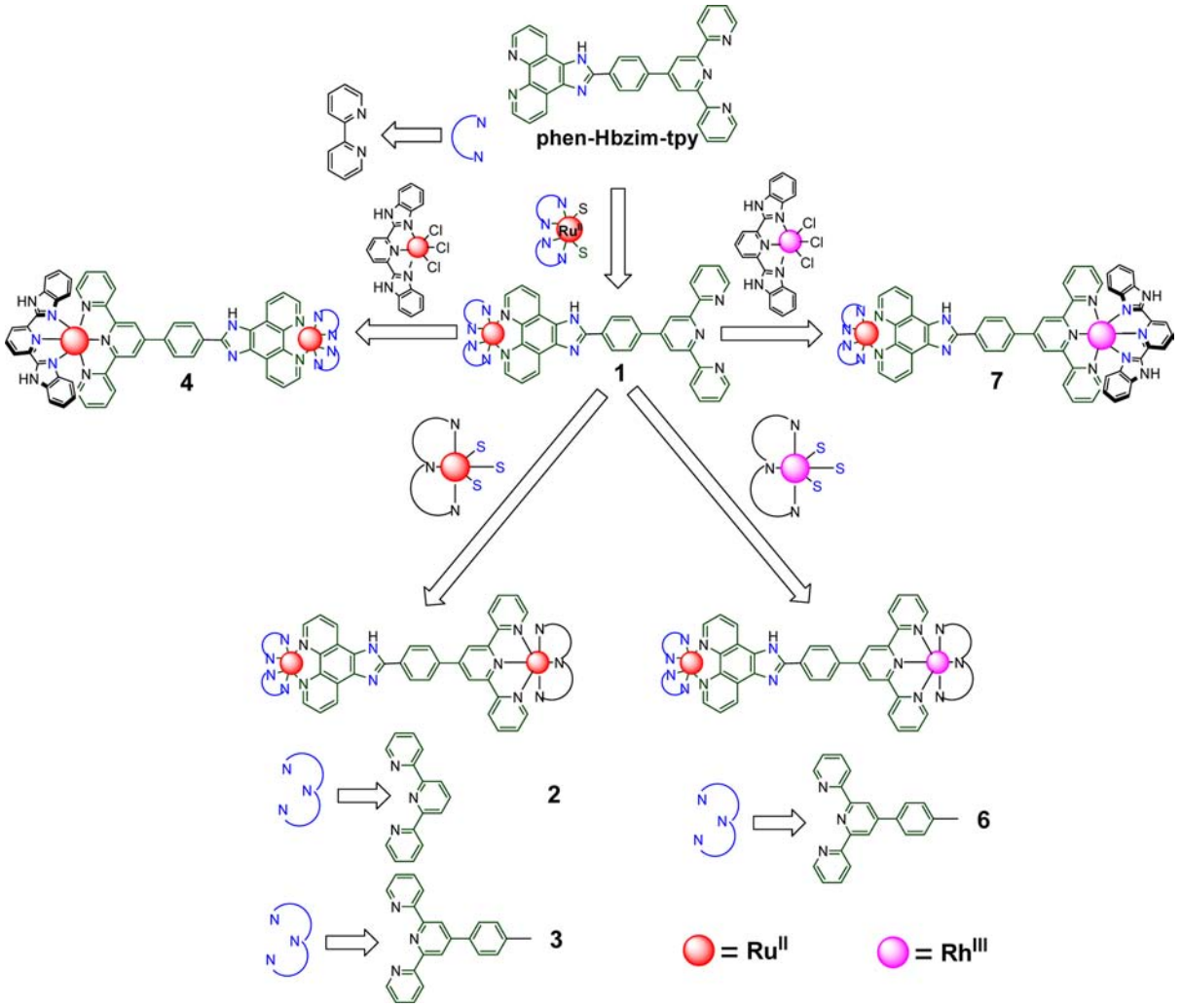

[(tpy-PhCH$_3$)RhCl$_3$] (75 mg, 0.14 mmol) and AgBF$_4$ (92 mg, 0.47 mmol) in acetone (30 mL) for 4 h and removing the AgCl precipitate. The filtrate was added slowly to a methanol−chloroform solution of phen-Hbzim-tpy (120 mg, 0.23 mmol), and the solution was refluxed for 3 h, during which time the color of the solution changed from light yellow to orange. Upon cooling, the yellow-orange compound that deposited was collected by filtration. The compound was purified by silica gel column chromatography using acetonitrile−water (10:1, v/v) as the eluent. The eluents were reduced to a small volume (∼5 mL) when a microcrystalline compound deposited. Further purification was carried out by recrystallization of the compound from a methanol−water (5:1, v/v) mixture in the presence of a few drops of aqueous 10^{-4} M perchloric acid (98 mg, yield 55%). Anal. Calcd for $C_{56}H_{44}N_{10}B_3F_{12}O_3Rh$: C, 53.03; H, 3.01; N, 11.04. Found: C, 53.01; H, 3.03; N, 11.02. ^{1}H NMR (300 MHz, DMSO-d_6, δ/ppm): 14.62 (s, 1H, NH imidazole), 9.25 (s, 2H, H3′), 9.21−9.18 (m, 6H, 2H3′ + 4H6), 9.09−9.05 (m, 2H, H9), 8.58−8.50 (m, 8H, 4H7 + 4H8), 8.21−8.17 (m, 6H, 4H4 + 2H11), 8.08−7.98 (m, 6H, 4H3 + 2H10), 7.52 (d, 4H, J = 8.1 Hz, H5), 2.48 (s, 3H, CH$_3$). ESI-MS (positive, CH$_3$CN): m/z 499.39 (100%) [(tpy-PhCH$_3$)Rh(phen-bzim-tpy)-(Na)]$^{3+}$. UV−vis [CH$_3$CN; λ_{max}/nm (ε/M^{-1} cm^{-1})]: 355 (20750), 315 (55420), 287 (59000).

[(bpy)$_2$Ru(phen-Hbzim-tpy)Rh(tpy-PhCH$_3$)](ClO$_4$)$_5$·4H$_2$O (**6**). To an ethanol solution (20 mL) of [(tpy-PhCH$_3$)Rh(EtOH)$_3$]$^{3+}$, generated from 75 mg (0.15 mmol) of [(tpy-PhCH$_3$)RhCl$_3$], was added a second ethanol solution (30 mL) of **1** (180 mg, 0.15 mmol). The solution was refluxed 10 h, after which it was allowed to evaporate slowly at room temperature. The microcrystalline product that deposited upon standing overnight was filtered. The compound was then purified by silica gel column chromatography using acetonitrile as the eluent. The eluents were reduced to a small volume (∼5 mL), and to it was then added an aqueous solution of NaClO$_4$·H$_2$O when a red crystalline compound deposited. Further purification was carried out by recrystallization of the compound from a mixture of MeCN and MeOH (1:5) in the presence of a few drops of aqueous 10^{-4} M perchloric acid (186 mg, yield 69%). Anal. Calcd for $C_{76}H_{62}N_{14}Cl_5O_{24}RuRh$: C, 47.13; H, 3.23; N, 10.12. Found: C, 47.10; H, 3.24; N, 10.14. ^{1}H NMR (300 MHz, DMSO-d_6, δ/ppm): 14.64 (s, 1H, NH imidazole), 9.71 (s, 2H, H3′), 9.62 (s, 2H, H3′), 9.27−9.25 (m, 4H, H6), 9.16 (br, 2H, H9), 8.87 (t, 4H, J = 9.5 Hz, H3″), 8.73 (nr, 4H, 2H7 + 2H8), 8.48−8.41 (m, 4H, 2H7 + 2H8), 8.23 (t, 4H, J = 7.7 Hz, H4), 8.13 (t, 4H, J = 7.2 Hz, H4′), 8.00 (t, 4H, J = 5.8 Hz, H6′), 7.86 (d, 4H, J = 5.2 Hz, 2H10 + 2H11), 7.67−7.59 (m, 8H, 4H3 + 4H5′), 7.37 (t, 4H, J = 6.4 Hz, H5), 2.52 (s, 3H, CH$_3$). ESI-MS (positive, CH$_3$CN): m/z 273.21 (100%) [(bpy)$_2$Ru(phen-Hbzim-tpy)Rh(tpy-PhCH$_3$)]$^{5+}$, 341.50 (57%) [(bpy)$_2$Ru(phen-bzim-tpy)Rh(tpy-PhCH$_3$)]$^{4+}$. UV−vis [CH$_3$CN; λ_{max}/nm (ε/M^{-1} cm^{-1})]: 460 (32500), 428 (sh, 30330), 370 (br, 56580), 288 (158330).

[(bpy)$_2$Ru(phen-Hbzim-tpy)Rh(H$_2$pbbzim)](ClO$_4$)$_5$·2H$_2$O (**7**). Starting from [(H$_2$pbbzim)RhCl$_3$], the preparation of **7** was the same as that described for **4**, except the temperature and refluxing time were 200 °C and 24 h, respectively. Yield: 55%. Anal. Calcd for $C_{73}H_{54}N_{16}Cl_5O_{22}RuRh$: C, 46.43; H, 2.88; N, 11.87. Found: C, 46.40; H, 2.90; N, 11.85. ^{1}H NMR (500 MHz, DMSO-d_6, δ/ppm): 15.07 (s, 1H, NH imidazole), 14.69 (s, 2H, NH imidazole), 9.83 (s, 2H, H3′), 9.18 (t, 4H, J = 8.7 Hz, H3″), 8.89 (d, 4H, J = 8.0 Hz, 2H6

dx.doi.org/10.1021/ic400449c | Inorg. Chem. 2013, 52, 7933−7946

+ 2H11′), 8.86 (d, 2H, J = 8.5 Hz, H9), 8.77 (d, 2H, J = 8.0 Hz, H8), 8.73 (d, 2H, J = 6.5 Hz, H7), 8.36 (t, 1H, J = 7.7 Hz, H10′), 8.24 (t, 2H, J = 7.7 Hz, 2H4), 8.22−8.15 (m, 6H, 4H4′ + 2H11), 8.00 (t, 2H, J = 6.2 Hz, 2H10), 7.88 (s, nr, 4H, H6′), 7.69 (d, 2H, J = 7.5 Hz, 2H3), 7.65 (d, 2H, J = 5.5 Hz, 2H12), 7.61 (t, 2H, J = 6.5 Hz, H5′), 7.58 (t, 2H, J = 6.5 Hz, H5′), 7.38 (t, 2H, J = 6.5 Hz, H5), 7.18 (s, nr, 2H, H13), 7.01 (s, nr, 2H, H14), 6.10 (d, 2H, J = 7.5 Hz, H15). ESI-MS (positive, CH_3CN): m/z 338.63 (18%) $[(bpy)_2Ru(phen\text{-}Hbzim\text{-}tpy)Rh(Hpbbzim)]^{4+}$, 451.16 (100%) $[(bpy)_2Ru(phen\text{-}Hbzim\text{-}tpy)Rh(pbbzim)]^{3+}$, 676.24 (68%)$[(bpy)_2Ru(phen\text{-}bzim\text{-}tpy)Rh(pbbzim)]^{2+}$. UV−vis [$CH_3CN$; λ_{max}/nm (ε/M^{-1} cm^{-1})]: 460 (25830), 386 (br, 48160), 332 (sh, 54410), 287 (141660).

Physical Measurements. Elemental (C, H, and N) analyses were performed on a Perkin-Elmer 2400II analyzer. Electrospray ionization mass spectra (ESI-MS) were obtained on a Micromass Qtof YA 263 mass spectrometer. ^{1}H and {^{1}H−^{1}H} COSY NMR spectra of the complexes were obtained either on a Bruker Avance DPX 300 MHz or a 500 MHz spectrometer using a DMSO-d_6 solution.

Electronic spectra were recorded on a Shimadzu UV-1800 spectrophotometer. To determine the pK_a values of the complexes, spectrophotometric titrations were carried out with a series of MeCN−aqueous buffer (3:2, v/v) solutions containing the same amount of complex (10^{-5} M) and the pH was adjusted in the range 2−12. A Robinson−Britton buffer was used in the study.[24] The pH measurements were made with a Beckman Research model pH meter. The pH meter responded reproducibly to variation of the hydrogen ion concentration, and as such, the pH meter readings were referred to as the pH. The individual pK values were evaluated from the two segments of the spectrophotometric titration data and using the equation

$$\mathrm{pH} = \mathrm{p}K - \log \frac{A - A_0}{A_f - A_0} \quad (1)$$

Steady-state emission spectra were recorded on a Perkin-Elmer LS55 fluorescence spectrophotometer. The room temperature spectra were obtained in acetonitrile solutions, while the spectra at 77 K were recorded in 4:1 (v/v) ethanol−methanol glass. Photoluminescence titrations were carried out with the same sets of solutions as those made with spectrophotometry. The quantum yields were determined by a relative method using $[Ru(bpy)_3]^{2+}$ as the standard.

$$\Phi_r = \Phi_{std} \frac{A_{std}}{A_r} \frac{I_r}{I_{std}} \frac{\eta_r^2}{\eta_{std}^2} \quad (2)$$

Time-correlated single-photon-counting (TCSPC) measurements were carried out for the luminescence decay of the complexes. For TCSPC measurement, photoexcitation was made at 440 nm using a picosecond diode laser (IBH Nanoled-07) in an IBH Fluorocube apparatus. The lifetimes of the complexes were also recorded as a function of the pH of the solution. The fluorescence decay data were collected on a Hamamatsu MCP photomultiplier (R3809) and were analyzed by using IBH DAS6 software.

The electrochemical measurements were carried out with a BAS epsilon electrochemistry system. A three-electrode assembly comprising a platinum or glassy carbon working electrode, a platinum auxiliary electrode, and a Ag/AgCl reference electrode was used. Cyclic voltammetric (CV) and square-wave voltammetric (SWV) measurements were carried out at 25 °C in an acetonitrile solution of the complexes (approximately 1 mM), and the concentration of the supporting electrolyte tetraethylammonium perchlorate was maintained at 0.1 M. The electrochemical measurements were carried out with oxygen-free solutions made by purging with purified nitrogen. The potentials measured were compensated for by the iR drop in the cell. Under the experimental condition used, the reversible oxidation of the ferrocene/ferrocenium ion was observed at 0.36 V. For variable-pH electrochemical measurements, a MeCN−aqueous (3:2, v/v) solution of the complexes was used. The $E_{1/2}$ value of the ferrocene/ferrocenium couple in the above solvent mixture at approximately pH 7 is 0.26 V.

Experimental uncertainties were as follows: absorption maxima, ±2 nm; molar absorption coefficients, 10%; emission maxima, ±5 nm; excited-state lifetimes, 10%; luminescence quantum yields, 20%; redox potentials, ±10 mV.

RESULTS AND DISCUSSION

Synthesis and Characterization of the Complexes. The general synthetic procedures for the homo- and heterobimetallic ruthenium(II) and rhodium(III) complexes are given in Scheme 1. The key monometallic ruthenium(II) compound $[(bpy)_2Ru^{II}(phen\text{-}Hbzim\text{-}tpy)]^{2+}$ has been prepared by a modification of the previously described procedure.[13] We have reported earlier that in terms of the reaction rate and yield the solvated cation $[(bpy)_2Ru(EtOH)_2]^{2+}$, generated by treating stoichiometric amounts of *cis*-$[(bpy)_2RuCl_2]$ and $AgClO_4$ in ethanol, acts as a better precursor relative to *cis*-$[(bpy)_2RuCl_2]$ itself.[12,18] Thus, the monometallic complex **1** was readily obtained by reacting $[(bpy)_2Ru(EtOH)_2]^{2+}$ with the bridging ligand phen-Hbzim-tpy in the ratio 1:1 in refluxing ethanol. As an alternative approach, the same compound was prepared previously by reacting phen-Hbzim-tpy directly with $[(bpy)_2RuCl_2]$.[13] However, the procedure took a considerably longer time. Moreover, in our procedure, as the resulting compound got precipitated upon cooling to room temperature, the purification process became simpler. This monometallic precursor complex containing a free terpyridine site is allowed to react with either $[(tpy/tpy\text{-}PhCH_3)RuL_3]$ or $[(tpy\text{-}PhCH_3)RhL_3]$ (L = ethanol) in refluxing ethanol for 6 h for the synthesis of the unsymmetrical homobimetallic ruthenium(II)−ruthenium(II) complexes and 10 h for the heterobimetallic ruthenium(II)−rhodium(III) compounds, respectively. $[(tpy/tpy\text{-}PhCH_3)RuL_3]$ or $[(tpy\text{-}PhCH_3)RhL_3]$ (L = acetone or ethanol) was obtained by first replacing the chloride ligands of the complexes $[(tpy/tpy\text{-}PhCH_3)RuCl_3]$ or $[(tpy\text{-}PhCH_3)RhCl_3]$ by solvent molecules using $AgBF_4$ in refluxing acetone and then rotary evaporating with ethanol. On the other hand, dehalogenation of the ruthenium(III) and rhodium(III) precursors $[(H_2pbbzim)RuCl_3]$ and $[(H_2pbbzim)RhCl_3]$ with $AgBF_4$ in acetone was far less efficient. Thus, both complexes $[(bpy)_2Ru^{II}(phen\text{-}Hbzim\text{-}tpy)Ru^{II}(H_2pbbzim)]^{4+}$ and $[(bpy)_2Ru^{II}(phen\text{-}Hbzim\text{-}tpy)Rh^{III}(H_2pbbzim)]^{5+}$ have been straightforwardly prepared by reacting $[(H_2pbbzim)RuCl_3]$ or $[(H_2pbbzim)RhCl_3]$ with **1** in ethylene glycol in the temperature range 180−200 °C, followed by anion metathesis with $NaClO_4$. All compounds were then purified by silica gel column chromatography using the appropriate eluent. Finally, the compounds were recrystallized from an acetonitrile−methanol (1:1, v/v) mixture in the presence of a few drops of aqueous 10^{-4} M perchloric acid to keep the imidazole NH proton(s) intact. The compounds were characterized by elemental (C, H, and N) analyses, ESI-MS, UV−vis, and ^{1}H NMR spectroscopic measurements, and the results are given in the Experimental Section. ESI-MS spectra of the complexes and their simulated isotopic patterns are shown in Figures S1−S6 (Supporting Information).

^{1}H NMR Spectra. The ^{1}H NMR spectra of the complexes have been recorded in DMSO-d_6 at room temperature, and the assignments made for the observed chemical shifts, according to the numbering (Figures S7 and S8, Supporting Information), are listed in the Experimental Section. The spectral assignments of the complexes have been made with the help of their {^{1}H−^{1}H} COSY NMR spectra (Figures S9 and S10, Supporting Information) and relative areas of the peaks and

dx.doi.org/10.1021/ic400449c | Inorg. Chem. 2013, 52, 7933−7946

Table 1. Spectroscopic and Photophysical Data of 1−7

		luminescence							
		298 K[a]						77 K[b]	
compound	absorption[a] λ_{max}/nm (ε/M^{-1} cm^{-1})	λ_{max}/nm	τ/ns	Φ/10^{-3}	$k_r/10^5$ s^{-1}	$k_{nr}/10^7$ s^{-1}	k_{en}/k_{et}[c]/s^{-1}	λ_{max}/nm	Φ
1	460 (19750), 426 (sh, 15330), 326 (br, 51330), 288 (112250)	607	151	297	19.59	0.46		589	0.31
2	486 (35660), 460 (sh, 32250), 365 (br, 35750), 332 (sh, 49660), 308 (sh, 71410), 286 (100750)	657	2.37, 15.68	1.54	6.42, 0.98	42.12, 6.36	5.71×10^7	650	0.26
3	492 (45160), 458 (br, 34580), 364 (br, 33830), 331 (br, 66160) 310 (sh, 99080), 286 (141160)	660	2.83, 18.42	4.02	14.20, 2.18	35.19, 5.40	4.77×10^7	645	0.30
4	480 (br, 33660), 425 (sh, 22580), 373 (br, 44000), 348 (sh, 79830), 334 (sh, 76750), 315 (sh, 78500), 286 (128160)	685	10.71, 76.75	10.57	9.81, 1.37	9.23, 1.28	6.44×10^6	678	0.33
5	355 (20750), 315 (55420), 287 (59000)	455	1.15, 3.52	78.08	679, 222	80.11, 26.19		442	0.15
6	460 (32500), 428 (sh, 30330), 370 (br, 56580), 288 (158330)	608	11.98, 148	105	88.15, 7.12	7.46, 0.66	1.56×10^5	590	0.32
7	460 (25830), 386 (br, 48160), 332 (sh, 54410), 287 (141660)	606	9.56, 69.67	24.40	25.52, 3.50	10.20, 1.40	7.75×10^6	588	0.25

[a]In CH_3CN. [b]MeOH−EtOH (1:4, v/v) glass. [c]k_{en} corresponds to the rate constant for energy transfer in **2**−**4**, while k_{et} corresponds to the rate constant for electron transfer in **6** and **7**.

taking into consideration the usual ranges of J values for bpy, tpy, tpy-PhCH$_3$, and H$_2$pbbzim.[12] The ^{1}H NMR spectra for complexes **1**−**4** are shown in Figure S7 (Supporting Information), while those for complexes **5**−**7** are presented in Figure S8 (Supporting Information). The ^{1}H NMR spectra of the complexes show the occurrence of a fairly large number of resonances, some of which are overlapped with each other.

As may be seen in Figures S7 and S8 (Supporting Information), all of the resonances in the complexes, barring three, occur in the range of 7.00−9.25 ppm. Of the three disparate signals, the one that appears as a singlet at 2.50 ppm in **3** and at 2.52 ppm in **6** (not shown in Figures S7 and S8, Supporting Information), accounting for three protons, is clearly due to −CH$_3$ protons of the coordinated tpy-PhCH$_3$ moiety. The second-highest field resonance, which appears as a doublet at 6.07 ppm for **4** and at 6.10 ppm for **7**, is attributable to H15 of the H$_2$pbbzim moiety, because this proton experiences maximum shielding due to the anisotropic ring-current effect of the adjacent pyridine rings. The third distinct signal, which is most downfield-shifted, is observed either as a singlet or as a broad feature in the region 14.67−15.07 ppm due to the imidazole NH proton(s) of the coordinated phen-Hbzim-tpy and H$_2$pbbzim ligands. The imidazole NH protons are profoundly downfield-shifted in all of the complexes due to hydrogen bonding with DMSO-d_6. In the case of **4** and **7**, the occurrence of two distinct NH signals is observed in the region between 14.67 and 15.07 ppm due to the presence of two different kinds of imidazole NH protons with different chemical environments. By a comparison of the chemical shifts of the NH protons of **1**−**3**, the peaks at 14.67 ppm in **4** and at 14.69 ppm in **7** can be attributed to NH of phen-Hbzim-tpy, while the peaks observed at 15.05 ppm in **4** and at 15.07 ppm in **7** are due to NH of H$_2$pbbzim.

It is of interest to note that the H3′ protons, which appear as a singlet at 8.89−8.79 ppm in **1**, are considerably shifted to a downfield region in both the homo- and heterobimetallic complexes when the free terpyridine site in **1** is coordinated with a second metal center (Ru^{II} and Rh^{III}). Moreover, the presence of two closely situated singlets at 9.54 and 9.43 ppm in **3** and at 9.71 and 9.62 ppm in **6** clearly indicates the two different chemical environments of the H3′ protons. It is also to be noted that the H3 proton of the tpy moiety of phen-Hbzim-tpy in the bimetallic complexes shifts to a significantly upfield region compared to the monometallic ruthenium(II) complex **1** because this proton lies above the shielding region of a pyridine ring of the other tpy capping ligand.

Absorption Spectral Studies. The absorption spectral characteristics of the homobimetallic ruthenium(II)−ruthenium(II) and heterometallic ruthenium(II)−rhodium(III) complexes were studied in acetonitrile solutions at room temperature, and spectral data are catalogued in Table 1. For purposes of comparison, the UV−vis absorption spectral behaviors of phen-Hbzim-tpy and monometallic model compounds **1** and **5** were studied under the same experimental conditions.

Figure 1 shows the UV−vis absorption spectra of equimolar solutions of the parent monometallic (**1**) and homobimetallic

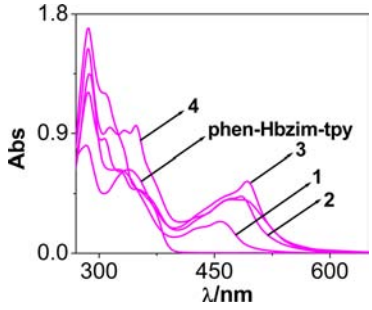

Figure 1. UV−vis absorption spectra of equimolar solutions of complexes **1**−**4** in acetonitrile at room temperature. The spectrum of phen-Hbzim-tpy in dimethylformamide−acetonitrile (1:9, v/v) is also included.

(**2**−**4**) ruthenium(II) complexes in acetonitrile. Complex **1** displays an electronic absorption spectrum containing bpy and phen-Hbzim-tpy $\pi \rightarrow \pi^*$ transitions at 288 and 326 nm and overlapping Ru(dπ) → bpy and Ru(dπ) → phen-Hbzim-tpy charge-transfer transitions (MLCT) between 426 and 460 nm. Previously, it was reported that bpy and phen-Hbzim-tpy $\pi \rightarrow \pi^*$ transitions occurred at 285 and 330 nm, while Ru(dπ) → bpy charge-transfer transitions (MLCT) occurred at 433 and 459 nm in 0.1 M sodium phosphate buffer (pH 6.8).[13] It is well-known that ruthenium(II) polypyridine complexes of this type typically display ligand-based $\pi \rightarrow \pi^*$ transitions from

dx.doi.org/10.1021/ic400449c | Inorg. Chem. 2013, 52, 7933−7946

each polypyridine ligand in the UV region of the spectrum and MLCT transitions for each acceptor ligand in the visible region.[1−4,12] In this broad-band system, the overlapping contributions from two types of ligands cannot be distinguished, although the expectation is that the MLCT transition involving the phen-Hbzim-tpy ligand should be at a slightly lower energy than those involving bpy ligands.

In the homobimetallic complexes, there is another intense MLCT band in the lower-energy region in addition to the MLCT bands for the monometallic complex **1**, and this can be assigned as Ru($d\pi$) → tpy/tpy-PhCH$_3$/phen-Hbzim-tpy charge-transition transition(s). The MLCT band in the range of 480−492 nm is typical of bis(terpyridine)ruthenium(II) complexes.[4,12] Upon coordination of a second Ru^{II} center to the parent monometallic complex **1**, substantial stabilization of the π^* orbital of phen-Hbzim-tpy occurs, and this stabilization is reflected in the red shift of the phen-Hbzim-tpy-based $\pi \rightarrow \pi^*$ transitions that now occur around 348 and 365 nm in the bimetallic complexes compared to 284 and 338 nm in free phen-Hbzim-tpy and at 288 and 326 nm in **1**.

The UV−vis absorption spectra of the heterobimetallic ruthenium(II)−rhodium(III) complexes (**6** and **7**) in an acetonitrile solution at room temperature are shown in Figure 2. For the purpose of comparison, the spectra of **1** and **5** are

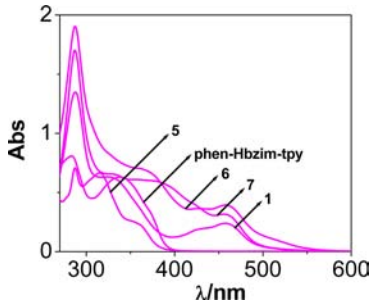

Figure 2. UV−vis absorption spectra of equimolar solutions of complexes of **1** and **5**−**7** in acetonitrile and of the ligand phen-Hbzim-tpy in dimethylformamide−acetonitrile (1:9, v/v) at room temperature.

also presented in Figure 2. Complex **5** does not absorb in the visible, whereas in the UV region, three principle bands with maxima at 355, 315, and 287 nm can be identified. The heterometallic complexes (**6** and **7**), on the other hand, show intense bands in both the visible and UV regions. For **6** and **7**, the lowest-energy MLCT band practically coincides with that of the ruthenium(II) model compound **1**. Thus, the visible region is characterized by the MLCT transitions of the ruthenium(II) component. The UV region is dominated by ligand-centered transitions of both the ruthenium(II) and rhodium(III) components. Comparison of the spectra of **6** and **7** with that of the rhodium(III) model complex (**5**) allows us to assign the shoulders at 370 nm for **6** and 386 nm for **7**, corresponding to the distinct features of the rhodium(III) polypyridyl (tpy/phen-Hbzim-tpy) component.[25,26] Thus, the absorption spectra of the heterobimetallic dyads are an approximate superposition of those of the mononuclear models. The substantial additivity of the spectroscopic properties of the molecular components in the ruthenium(II)−rhodium(III) binuclear complexes (**6** and **7**), investigated in this study points toward a relatively weak degree of metal−metal electronic coupling.[27−29]

Luminescence Spectral Studies. The photoluminescence spectral behaviors of the complexes were studied in acetonitrile solutions at room temperature and at 77 K in ethanol−methanol (4:1, v/v) glass. Table 1 summarizes the emission maxima, quantum yields, and lifetimes of homo- and heterobimetallic complexes. The emission properties of the model complexes **1** and **5** are also reported in Table 1. Figure 3

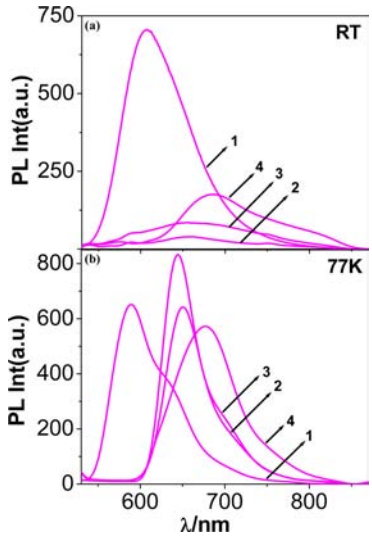

Figure 3. Photoluminescence spectra of **1**−**4** at room temperature in acetonitrile (a) and at 77 K in methanol−ethanol (1:4, v/v) glass (b).

compares the photoluminescence spectra of equimolar solutions of homobimetallic ruthenium(II) complexes **2**−**4**, along with the monometallic precursor complex **1** at both room temperature and 77 K. Complex **1** displays a luminescence spectrum with its maximum at 607 nm at room temperature and at 589 nm at 77 K. Complex **1** was reported to be emissive at room temperature with an emission maximum at 604 nm and a lifetime of 812 ns in 0.1 M sodium phosphate buffer (pH 6.8),[13] typical of the ruthenium(II) polypyridine family.[1−4] The unsymmetrical bimetallic ruthenium(II) complexes (**2**−**4**), on the other hand, upon excitation at their MLCT absorption maxima, display a broad emission maximum in the range of 657−685 nm at room temperature and between 645 and 678 nm at 77 K. Luminescence in these complexes also occurs from an MLCT state, which is, by comparison with a large number of closely related complexes, predominantly triplet in character.[1−4,12] Upon coordination of a second Ru^{II} center to the remote tpy site of the bridging phen-Hbzim-tpy ligand, the emission maximum in all of the bimetallic complexes is red-shifted with concomitant quenching of the emission intensity relative to the monometallic complex. The less intense and lower-energy emission of the unsymmetrical bimetallic complexes is explained by the presence of a Ru(tpy)$_2$-type chromophore. The small energy difference between ^{3}MLCT and ^{3}MC states in ruthenium(II) tridentate polypyridine complexes compared to the bidentate ligands is due to an ill-fitted octahedral arrangement, which, in turn, is responsible for the poor room temperature luminescence properties of Ru(tpy)$_2$-type complexes.[4,12] Upon going from a fluid solution to frozen glass, the emission maxima get blue-shifted with significant increases of the intensities and quantum yields, which are the characteristics of typical MLCT emitters.[1−4,12,18] At 77 K, each spectrum displays a well-defined vibronic

dx.doi.org/10.1021/ic400449c | Inorg. Chem. 2013, 52, 7933−7946

progression in the lower-energy region with spacing of ~1401 cm^{-1} for **1**, ~1418 cm^{-1} for **2**, ~1403 cm^{-1} for **3**, ~1438 cm^{-1} for **4**, ~1102 cm^{-1} for **6**, and ~1234 cm^{-1} for **7**, which are similar to those reported for $[M(bpy)_3]^{2+}$, $[M(tpy)_2]^{2+}$ (M = Ru^{II} and Os^{II}), and the other polypyridine complexes of ruthenium(II) and osmium(II) and can be attributed to aromatic stretching vibrations of the ligands.[19,21] For a better understanding of the complete kinetic schemes of the excited-state deactivation of these complexes at lower temperatures, detailed temperature-dependent lifetime measurements including those at 77 K will be required. Unfortunately, because of the lack of such a facility, we are unable to address this issue presently.

Photoluminescence spectra of ruthenium(II)−rhodium(III) complexes (**6** and **7**) as well as **1**, obtained upon visible MLCT excitation on their absorbance-matched solutions at room temperature as well as at 77 K, are presented in Figure 4. It is

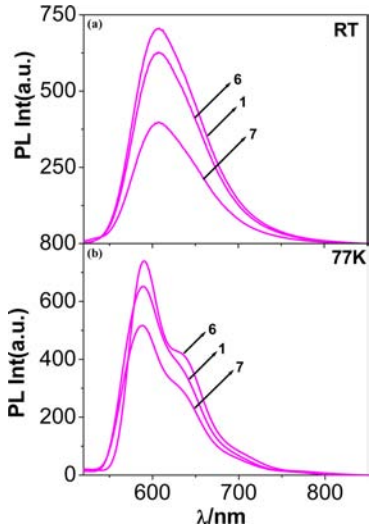

Figure 4. Photoluminescence spectra of **1**, **6**, and **7** at room temperature in acetonitrile (a) and at 77 K in methanol−ethanol (1:4, v/v) glass (b).

observed that an emission maximum at 608 nm for **6** and at 606 nm for **7** at room temperature and at 590 nm for **6** and at 588 nm for **7** at 77 K is observed for both heterometallic dyads close to that of the ruthenium(II) model compound **1**. Thus, both ruthenium(II)−rhodium(III) complexes were found to exhibit ruthenium-based emission. The excitation spectra of the ruthenium(II)-based emission for the heterometallic dyads matched very closely to their absorption spectra. Again a comparison of the luminescence intensity and quantum yield of **1** with those of **6** and **7** indicates that significant quenching of the ruthenium(II)-based emission occurs in both heterometallic dyads.

Electrochemical Properties. The electrochemical behaviors of homo- and heterometallic complexes were studied by CV and SWV in an acetonitrile solution at room temperature. For the purpose of comparison, the electrochemical behaviors of the monometallic model compounds (**1** and **5**) were also studied under the same experimental conditions. The relevant electrochemical data are summarized in Table 2.

Complex **1** is found to undergo one reversible oxidation at 1.31 V and in the positive potential window (0 to +1.6 V) and four successive quasi-reversible or irreversible reductions in the

Table 2. Electrochemical Data[a] for 1−7 in Acetonitrile

compound	oxidation[b] $E_{1/2}$(ox)/V	reduction[c] $E_{1/2}$(red)/V
1	1.31	−1.34, −1.53, −1.78, −1.90
2	1.33	−1.19, −1.34, −1.43, −1.55, −1.89, −2.17
3	1.32	−1.16, −1.34, −1.55, −1.88, −2.15
4	1.36, 1.12	−1.13, −1.36, −1.50, −1.90, −1.98
5		−0.75, −1.20, −1.55, −1.99
6	1.33	−0.70, −1.34, −1.56, −1.88, −2.13
7	1.37	−0.61, −1.18, −1.35, −1.55, −1.85

[a]All potentials are referenced against the Ag/AgCl electrode with $E_{1/2}$ = 0.36 V for a Fc/Fc^+ couple. [b]Reversible electron-transfer process with a platinum working electrode. [c]$E_{1/2}$ values obtained from SWV using a glassy carbon electrode.

negative potential window (0 to −2.0 V) (Figures S11 and S12, Supporting Information). In ruthenium(II) polypyridyl complexes, the highest occupied molecular orbital (HOMO) is normally localized on the metal center and oxidative processes are therefore metal-based, whereas the lowest unoccupied molecular orbital (LUMO) is usually ligand-based and the reduction processes are therefore ligand-centered, in agreement with literature data and the reversibility of most of the processes.[1−4] Thus, the oxidation at 1.31 V for **1** can been assigned as a Ru^{II}/Ru^{III} process. Previously, an irreversible oxidation behavior was reported in 0.1 M sodium phosphate buffer (pH 6.8) for **1**.[13] Reductively, it displays four couples because of the successive reductions of both phen-Hbzim-tpy and bpy ligands.

The homobimetallic complexes except **4** also exhibit one reversible oxidation at slightly more positive potential compared with **1** and five successive quasi-reversible or irreversible reductions in the negative potential window (0 to −2.3 V) (Figures S11 and S12, Supporting Information). Thus, the reversible oxidation at 1.33 V for **2** and at 1.32 V for **3** against the Ag/AgCl reference electrode has been assigned as a simultaneous two-electron Ru^{II}/Ru^{III} oxidation process. This is quite obvious because the distance between the two Ru^{II} centers is quite large. Complex **4**, on the other hand, displays two successive reversible one-electron oxidations at 1.36 and 1.12 V, with the ruthenium bound to the tpy site of the phen-Hbzim-tpy ligand oxidizing at lower potential. It is of interest to note that when the tpy site of the phen-Hbzim-tpy ligand in **1** is coordinated to another Ru^{II} center to form bimetallic complexes, stabilization of the phen-Hbzim-tpy π^* orbital is observed. This leads to a shift to the more positive potential of the phen-Hbzim-tpy-centered reductions.

The square-wave voltammogram of the rhodium(III) model compound **5** shows four successive reduction waves in the cathodic region (Figure S13, Supporting Information). The first reduction process occurring at −0.75 V can be assigned as the reduction of the Rh^{III} center by comparing the reduction potentials of other rhodium(III) polypyridine complexes.[25−27] The poorly reversible character of this process is as expected on the basis of the general redox behavior of rhodium(III) polypyridine complexes.[29,30] The remaining reduction couples are due to the successive reductions of both phen-Hbzim-tpy and bpy ligands as expected.

The heterobimetallic ruthenium(II)−rhodium(III) complexes **6** and **7** exhibit one reversible oxidation and five successive quasi-reversible reductions (Figures S13 and S14, Supporting Information). In the anodic region, oxidation of the

dx.doi.org/10.1021/ic400449c | Inorg. Chem. 2013, 52, 7933−7946

Ru^{II} center occurs at slightly more positive (1.33 V for **6** and 1.37 V for **7**) potential compared with **1**. The first reduction occurring at −0.70 V for **6** and at −0.61 V for **7** is quasi-reversible, and the reversibility of both couples increases as the scan rate is increased. By a comparison of the reduction potential (−0.75 V) of the model compound **5** and taking into account the irreversibility and the higher peak current for this peak relative to the ruthenium oxidation, it can be concluded that the first reduction corresponds to the Rh^{III}/Rh^{I} couple in both **6** and **7**. The Rh^{III}/Rh^{I} couple is expected to be irreversible because of generation of the d^8 rhodium(I) species, which would prefer to be square planar and is thus expected to undergo subsequent ligand loss.[29] Both complexes also display five successive reductions up to −2.3 V and can be assigned as the reductions of phen-Hbzim-tpy as well as bpy/tpy-$PhCH_3$/H_2pbbzim ligands. Thus, the electrochemical data indicate that the mixed-metal systems (**6** and **7**) possess a ruthenium-based HOMO and a rhodium-based LUMO. This would suggest that, although the lowest-lying spectroscopic transition seen in the electronic absorption spectroscopy of the heterometallic complexes was a Ru → polypyridine charge-transfer transition, excitation of these molecules to this state should be followed by intramolecular electron transfer to the lower-energy rhodium acceptor orbital. Because both **6** and **7** have a [(bpy)Ru^{II}(phen-Hbzim-tpy)] chromophore, which has been shown to be emissive at room temperature, it should be possible to use emission spectroscopy and emission lifetime measurements to probe the intramolecular electron-transfer quenching of the Ru → polypyridine charge-transfer excited state by the rhodium-based electron acceptor.[27−29]

Intercomponent Energy Transfer in Unsymmetrical Homobimetallic Ruthenium(II) Complexes. As was already mentioned, the emission intensity, quantum yield, and lifetime of the Ru^{II}-centered emission in all three bimetallic ruthenium(II) complexes (**2**−**4**) are considerably less compared to those of the monometallic parent compound **1**. This indicates that the second Ru^{II} center coordinated to the tpy site of phen-Hbzim-tpy probably induces a quenching effect on the [$(bpy)_2Ru^{II}$(phen-Hbzim-tpy)]-centered component. In principle, two predominant paths exist for the quenching of $[(bpy)_2Ru(phen\text{-}Hbzim\text{-}tpy)]^{2+}$-based luminescence in the unsymmetrical bimetallic complex: reductive electron-transfer quenching of the $[(bpy)_2Ru(phen\text{-}Hbzim\text{-}tpy)]^{2+}$-based excited state by the Ru^{II} center of the [(tpy/tpy-$PhCH_3$/H_2pbbzim)-Ru(phen-Hbzim-tpy)]$^{2+}$ component of the molecule and electronic energy transfer from the $[(bpy)_2Ru(phen\text{-}Hbzim\text{-}tpy)]^{2+}$ chromophore to the tpy-containing chromophore. We have estimated the extent of luminescence quenching of the $[(bpy)_2Ru(phen\text{-}Hbzim\text{-}tpy)]^{2+}$ chromophore by measuring the luminescence intensities of equimolar solutions of three bimetallic ruthenium(II) complexes as well as the monometallic parent compound **1**, keeping identical experimental conditions in all cases. The result obtained shows that about 99% of the luminescence intensity of the $[(bpy)_2Ru(phen\text{-}Hbzim\text{-}tpy)]^{2+}$ chromophore is quenched by the tpy-containing chromophore [(tpy/tpy-$PhCH_3$/H_2pbbzim)Ru(phen-Hbzim-tpy)]$^{2+}$ in the unsymmetrical bimetallic complexes **2**−**4**. The excited-state energy of the [$(bpy)_2Ru$(phen-Hbzim-tpy)]-based component is 2.10 eV, while that of the [(tpy/tpy-$PhCH_3$/H_2pbbzim)Ru-(phen-Hbzim-tpy)]-based component lies in the range of 1.83−1.92 eV, estimated from the emission maxima at 77 K in the complexes (Figure 3b). Therefore, the free-energy change for energy transfer from an excited-state [$(bpy)_2Ru$(phen-Hbzim-tpy)]-based component to a ground-state [(tpy/tpy-$PhCH_3$/H_2pbbzim)Ru(phen-Hbzim-tpy)]-based component lies in the range of −0.18 to −0.27 eV. This thermodynamically favored process accounts for the observed quenching.

The quenching, in principle, can take place by an electron-transfer process also. However, to be feasible, the process has to be thermodynamically favorable. The photoinduced oxidative quenching in the unsymmetrical bimetallic complexes **2**−**4**

$$*[(bpy)_2Ru^{II}(phen\text{-}Hbzim\text{-}tpy)Ru^{II}(tpy)]^{4+} \rightarrow [(bpy)_2Ru^{III}(phen\text{-}Hbzim\text{-}tpy)Ru^{I}(tpy)]^{4+}$$

$$\Delta G^\circ = E^\circ([(bpy)_2Ru^{II}(phen\text{-}Hbzim\text{-}tpy)Ru^{II}(tpy)]^{5+}/[(bpy)_2Ru^{II}(phen\text{-}Hbzim\text{-}tpy)Ru^{II}(tpy)]^{4+}) - E^\circ([(bpy)_2Ru^{II}(phen\text{-}Hbzim\text{-}tpy)Ru^{II}(tpy)]^{4+}/([(bpy)_2Ru^{II}(phen\text{-}Hbzim\text{-}tpy^{\bullet-})Ru^{II}(tpy)]^{3+} - E^{\circ\circ} \quad (3)$$

is highly unfavorable because the free energy change according to eq 3 is too high, lying in the range between +0.38 and +0.42 eV. Thus, evaluation of the redox potentials (Table 2) and excited-state energies of the unsymmetrical bimetallic complexes suggests that the electron-transfer process is energetically uphill, while the excitation energy transfer is exergonic.

The luminescence decay profiles of the three unsymmetrical bimetallic and monometallic precursor complexes in acetonitrile at room temperature are shown in Figure S15 (Supporting Information). The room temperature luminescence decays of the donor−acceptor complexes are double exponentials on both the red and blue edges of the emission compared with the monoexponential decay of the parent monometallic complex **1**. All three bimetallic complexes (**2**−**4**) also possess shorter excited-state lifetimes than the parent monometallic complex **1**. The rate constant k_{en} for energy transfer can be calculated using eq 4

$$k_{en} = 1/\tau - 1/\tau^0 \quad (4)$$

where τ^0 is the emission lifetime of the monometallic precursor complex **1** (151 ns) and τ is the luminescence lifetime of the unsymmetrical bimetallic complexes (15.7−76.8 ns). Thus, the values of k_{en} at room temperature lie in the range of 6.4×10^6−5.7×10^7 s^{-1}. The reason for such fast energy transfer is likely due to overlap between the donor emission and acceptor absorption. The energy-transfer process is also very efficient in low-temperature glasses. The structured luminescence characteristic of the $[(bpy)_2Ru(phen\text{-}Hbzim\text{-}tpy)]^{2+}$ chromophore is absent in the spectrum of the bimetallic complexes **2**−**4**. In the literature, intramolecular energy transfer of several types of unsymmetrical bimetallic ruthenium(II) complexes derived from heteroditopic bpy-tpy-type ligands has been reported.[31] Energy-transfer processes occur in two ways, viz., Dexter-type[32] through-bond electron exchange or Förster-type[33] through-space Coulombic interaction. However, in most cases, it is not easy to ascertain which particular mechanism plays the dominant role. Electron exchange becomes important where the spacer is either highly conjugated or relatively short, while the Coulombic mechanism becomes important when either the spacer is saturated or the transition dipoles are well-separated.[34]

Photoinduced Electron Transfer in the Heterobimetallic Ruthenium(II)−Rhodium(III) Complexes. A comparison of the emission intensity and quantum yield of the model

dx.doi.org/10.1021/ic400449c | Inorg. Chem. 2013, 52, 7933−7946

monometallic ruthenium(II) complex **1** with those of the heterometallic ruthenium(II)−rhodium(III) complexes **6** and **7** indicates that significant quenching of the ruthenium(II)-based emission occurs in both heterometallic dyads. The energy of the MLCT triplet state is 2.26 eV for **6** and 2.30 eV for **7**, estimated from the energies at the intersection point of the absorption and emission band of the dyads at room temperature. The energy of the intercomponent charge-transfer state can be obtained from electrochemical data of the dyads as the difference in the potentials for oxidation of Ru^{II} and for reduction of Rh^{III}.[27−29] Thus, values of 2.03 eV for **6** and 1.98 eV for **7** are obtained from the redox data for the energy of the charge-transfer state. No correction for electrostatic work terms is required in this case because of the charge shift character ($*Ru^{II}-Rh^{III} \rightarrow Ru^{III}-Rh^{II}$) of the process involved. Thus, the driving force for electron-transfer quenching from the ^{3}MLCT state ($*Ru^{II}-Rh^{III}$) to the electron-transfer state ($Ru^{III}-Rh^{II}$) is −0.23 eV for **6** and −0.32 eV for **7**. The emission lifetimes of the dyads were also measured at room temperature, and the observed decays for the complexes are presented in Figure S15, Supporting Information. For both dyads studied, the emission decay was biexponential, involving a short-lived minor component and a longer-lived major component. The excited-state lifetimes of **6** and **7** are 148 and 69.67 ns, respectively, compared to 151 ns for **1**. The rate constant of photoinduced electron transfer (k_{et}) can be calculated using eq 5.

$$k_{et} = 1/\tau([(bpy)_2Ru(phen\text{-}Hbzim\text{-}tpy)Rh(tpy\text{-}PhCH_3)]^{5+} - 1/\tau([(bpy)_2Ru(phen\text{-}Hbzim\text{-}tpy)]^{2+} \quad (5)$$

This allows us to calculate k_{et} for **6** as 1.56×10^5 s^{-1} and that for **7** as 7.75×10^6 s^{-1}.

The emission properties of heterometallic dyads were also studied in a rigid matrix at 77 K (4:1 EtOH−MeOH). Both complexes exhibit a structured MLCT emission with a maximum centered around 590 nm, and no quenching of the typical MLCT ruthenium-based emission takes place, clearly indicating that the electron-transfer process does not occur under these experimental conditions. This behavior is in line with what is expected to occur for processes that are slightly exergonic in fluid solution.[27,28]

pH-Induced Modulation of the Photophysical Properties of the Complexes. Upon coordination of the metal center(s) to the bridging phen-Hbzim-tpy ligand, imidazole NH proton(s) of phen-Hbzim-tpy as well as the terminal H_2pbbzim ligand in the complexes became appreciably acidic. Inasmuch as the imidazole NH group becomes appreciably acidic, we have been interested in studying the influence of the pH on the absorption, steady-state, and time-resolved emission behaviors of the complexes.

Spectrophotometric Studies of Protonic Equilibria. Spectrophotometric titrations of the complexes have been studied quantitatively in acetonitrile−water (3:2, v/v) solutions over the pH range 2.5−12. The spectral changes that occur for **2** and **3** with variation of the pH are shown in Figures 5 and S16 (Supporting Information).

It is clear that both complexes underwent two successive deprotonation processes over the pH range 2.5−12.0. Upon an increase of the pH of **3** from 2.5 to 7.5, the band at 495 and 310 nm and the valley at 400 nm decreased, while the shoulder at 353 nm increased slightly in intensity with the appearance of two isosbestic points at 373 and 328 nm. The second

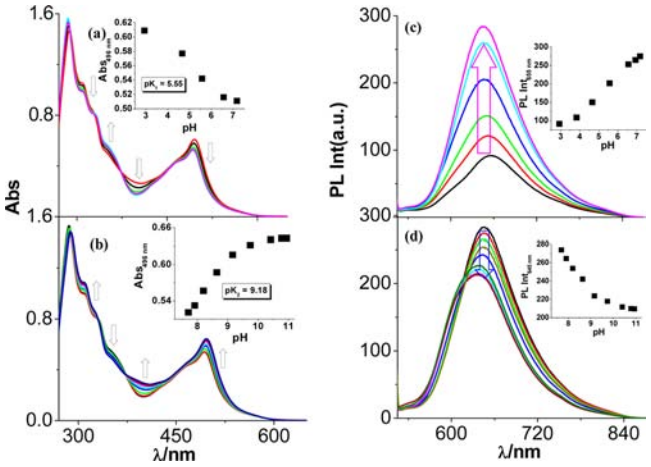

Figure 5. Changes in the absorption (a and b) and photoluminescence spectra (c and d) of **3** with variation of the pH in acetonitrile−water (3:2, v/v). The insets show the change of absorbance (a and b) and luminescence (c and d) with the pH.

deprotonation process occurred between pH 7.50 and 11.00, accompanying the following spectral features: the intensities of the MLCT band at 493 nm and the valley at 398 nm increased along with a small red shift, while the intensities of the band at 352 nm decreased. During the second deprotonation processes, the successive absorption curves passed through two new isosbestic points appearing at 372 and 330 nm. The first spectral change observed between pH 2.5 and 7.5 is probably due to dissociation of the protons on the protonated imidazole ring, while the second step can be assigned to deprotonation of the proton on the neutral imidazole ring, as shown in Scheme 2.

It is of interest to see the spectral changes for **4** because it has a more complicated structure with respect to having different types of NH protons with different chemical environments compared to the above two complexes. The spectral changes that occur for **4** as a function of the pH are shown in Figure 6. At first, upon an increase of the pH from 2.5 to 6.0, the band at 480 nm decreased slightly in intensity and two isosbestic points at 430 and 504 nm appeared; the spectral changes observed here are due to dissociation of one proton from the protonated imidazole ring. As the pH is increased from 6.0 to 6.6, the absorption maximum at 494 nm is progressively red-shifted to 511 nm, with isosbestic points arising at 510, 421, and 357 nm; upon further increases of the pH between 6.6 and 7.6, the bands are additionally red-shifted through a new set of isosbestic points at 520 and 440 nm until the maximum at 514 nm appeared at pH 7.6. Thus, these second and third deprotonation processes indicate that the two NH protons associated with the H_2pbbzim moiety are successively deprotonated in the pH range 6.0−7.6. The last deprotonation step occurred between pH 7.60 and 10.50 probably because of deprotonation of the neutral imidazole NH proton associated with the phen-Hbzim-tpy moiety.

Upon close inspection of the changes in the spectral profiles with increases of the pH, the occurrence of four successive deprotonation steps becomes evident, as shown in Scheme 3 over the pH range 2.5−12.0.

The changes that occur for **6** over the pH range 2.5−12.0 are shown in Figure S17 (Supporting Information). Similar to **2** and **3**, this complex also undergoes two successive deprotona-

dx.doi.org/10.1021/ic400449c | Inorg. Chem. 2013, 52, 7933−7946

Scheme 2

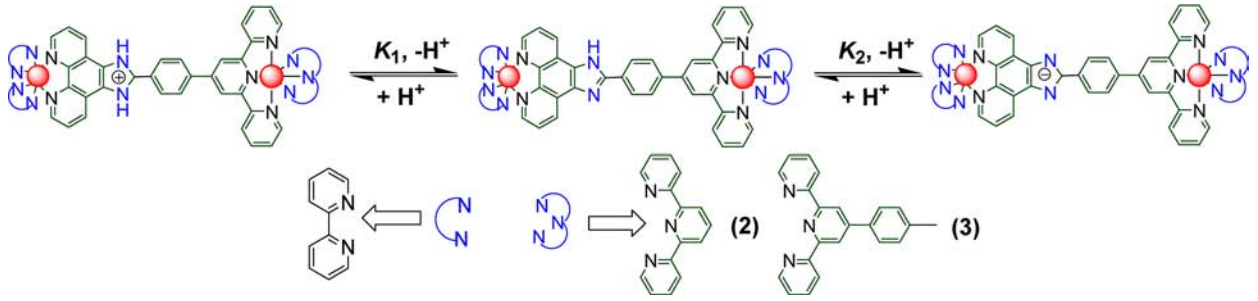

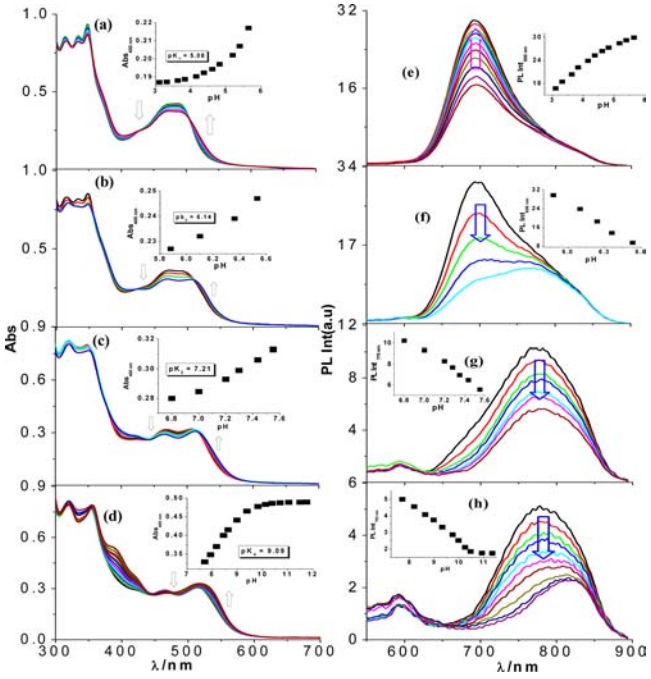

Figure 6. Changes in the absorption (a–d) and photoluminescence (e–h) spectra of **4** with variation of the pH in acetonitrile–water (3:2, v/v). The insets show the change of absorbance (a–d) and luminescence (e–h) with the pH.

tion processes over the pH range 2.5–12.0, as shown in Scheme 2.

Finally, the absorption spectral changes that occur for **7** with variation of the pH are shown in Figure 7. In contrast to **4**, the complex underwent three successive deprotonation processes over the pH range 2.5–12.0. As expected, the first step is due to deprotonation of the protonated imidazole NH of the phen-Hbzim-tpy moiety. It is to be noted that dissociation of this proton occurred at a lower pH compared with that of **4** because of the increased positive charge on the complex. In contrast to **4**, dissociation of two NH protons of the H_2pbbzim moiety occurs in a single step. The last deprotonation step is again from the neutral imidazole moiety associated with the phen-Hbzim-tpy ligand.

The individual p*K* values of complexes **2**–**4**, **6**, and **7** have been evaluated using eq 1 from the different segments of the spectrophotometric titration data and are presented in Table 3. Clearly, the p*K* values of the heterometallic complexes **6** and **7** are less compared with their homometallic analogues **2**–**4** because of the relatively more electron-withdrawing nature of rhodium(III) than that of ruthenium(II). It is of interest to note that, with deprotonation of the coordinated azole ligands, red shifts of the MLCT bands occur to some extent for all complexes. This is an expected trend because, with an increase of the electron density at the metal center due to the azole ligand deprotonation, it becomes easier to transfer an electron to the acceptor π * orbitals of the polypyridine ligands.

Scheme 3

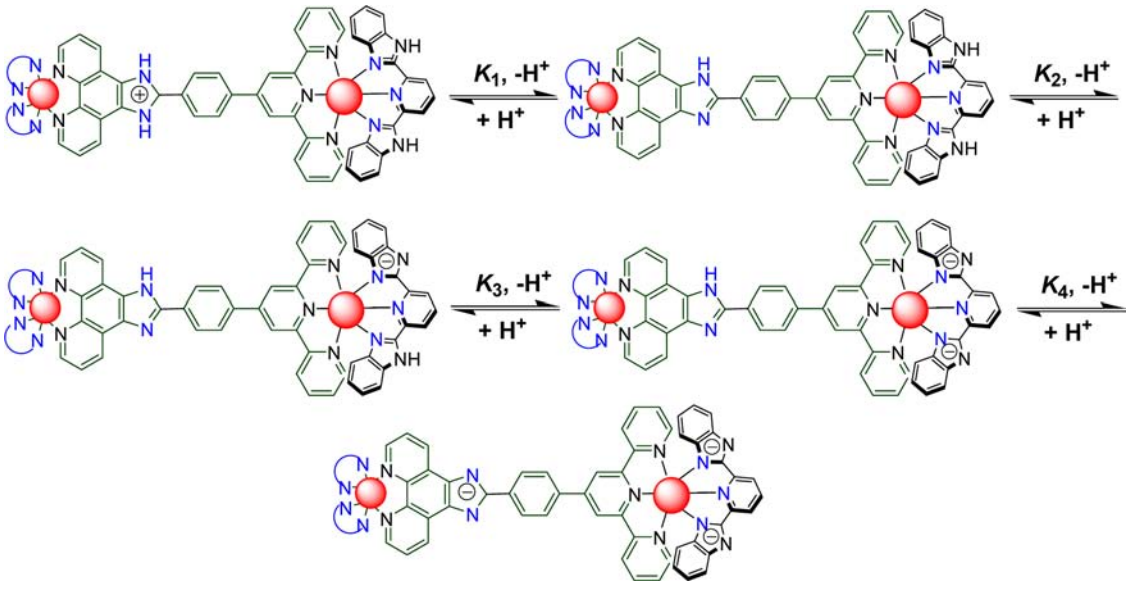

dx.doi.org/10.1021/ic400449c | *Inorg. Chem.* 2013, 52, 7933–7946

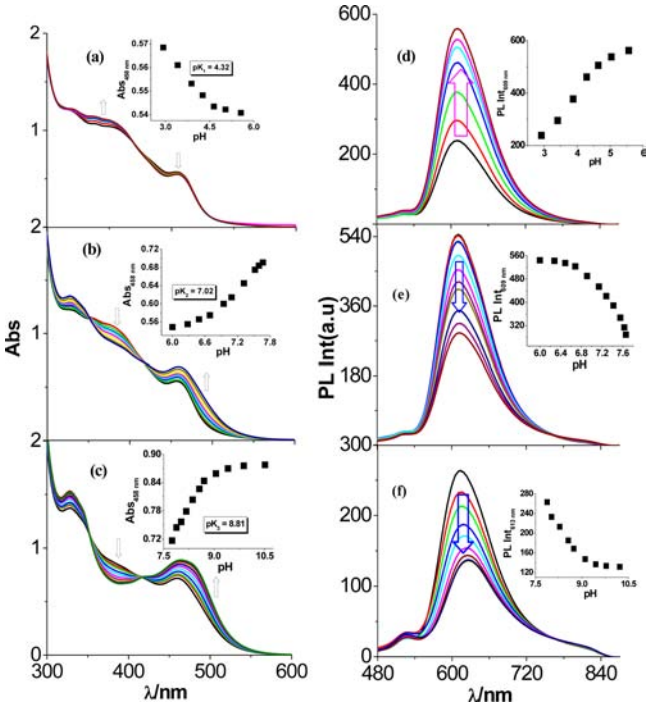

Figure 7. Changes in the absorption (a–c) and photoluminescence (d–f) spectra of **7** with variation of the pH in acetonitrile–water (3:2, v/v). The insets show the change of absorbance (a–c) and luminescence (d–f) with the pH.

Spectrofluorometric Studies of Protonic Equilibria. It has been observed that deprotonation of the imidazole NH protons of the complexes shifts the MLCT bands to higher wavelengths, and it has been of interest to us to find out the extent of changes that occur in the excited states of the complexes upon deprotonation. Photoluminescence titrations of the homo- and heterobimetallic complexes with variation of the pH were carried out in the same way as was already described for spectrophotometric measurements.

The effect of the pH on the luminescence spectra of **2** and **3** is already shown in Figures 5 and S16 (Supporting Information). When the pH is increased from 2.5 to 7.5, significant increases in the emission intensities occur (Figures 5c and S16c, Supporting Information) in both complexes. On the other hand, upon increasing the pH from 7.5 to 12.0, the emission intensities were found to decrease gradually with a small blue shift of the emission maximum. Thus, the emission versus pH profile consists of two reverse profiles corresponding to two successive excited-state deprotonation processes of the coordinated phen-Hbzim-tpy moiety in the complexes over the pH region from 2.5 to 12.0. It is of interest to note that the complex acted as an "off–on" emission switch with an emission enhancement factor of ~3.0 over the pH region of 2.5–7.5. On the contrary, the same complex acted as "on–off" emission switch with an emission quenching factor of ~1.4 over the pH range of 7.5–12.0.

Parts e–h in Figure 6 show the effects of variation of the pH on the luminescence spectral profiles of **4**. Similar to the absorption spectra, photoluminescence spectral profiles also show that the complex underwent four successive deprotonation processes over the pH range 2.5–12.0. When the pH is increased from 2.5 to 6.0, an increase in the emission intensity at 693 nm occurs (Figure 6e). On the other hand, upon an increase in the pH from 6.0 to 12.0, the emission intensities of the complex were found to decrease gradually in three successive steps (Figure 6f–h), with the emission maximum red-shifted from 693 to 818 nm. Complete quenching of the luminescence intensity of the complex occurs at pH ~11.00.

The effect of an increase of the pH on the luminescence spectrum of **6** is shown in Figure S17c,d (Supporting Information), and the inset shows enhancement and quenching of the luminescence intensity at 612 nm as function of the pH of the solution. Again, similar to the bimetallic ruthenium(II) complexes, it is seen that, in the low pH range of 2.5–6.0, enhancement of the luminescence intensity of the band at 612 nm occurs. On the other hand, upon an increase of the pH from 6.0 to 12.0, the emission intensities were found to decrease gradually, with the emission maximum red-shifted from 612 to 624 nm. Thus, the emission versus pH profile in this case again consists of two reverse profiles corresponding to two successive excited-state deprotonation processes of the coordinated phen-Hbzim-tpy moiety in the complexes over the pH region from 2.5 to 12.0.

The emission spectral changes of **7** as a function of the pH are shown in Figure 7d–f. Upon an increase of the pH from 2.5 to 5.5, the intensity of the emission maximum at 610 nm increased by about 131%. By contrast, when the pH is increased from 5.5 to 7.8, a significant decrease (48%) of the emission intensities occurs around 610 nm. Upon a further increase of the pH from 7.8 to 9.5, again a sharp decrease in the emission intensity was observed and the emission maximum was slightly red-shifted from 610 to 625 nm. Clearly, the emission spectral changes are associated with three excited-state deprotonation processes, and each of the processes dealt with the same proton(s) as UV–vis spectral titrations. The changes of the relative intensities versus pH are shown in the insets of Figure 7d–f.

The effect of the pH on the luminescence lifetimes of the complexes is shown in Figures 8 and S18–S21 (Supporting Information). All bimetallic complexes exhibited biexponential decays compared with the monoexponential decay for the parent monometallic ruthenium(II) complex **1**. The lifetime versus pH profiles of all complexes consist of two reverse profiles over the pH range 2.5–12.0. When the pH is increased from 2.5 to 7.5, an increase in the luminescence lifetimes occurs

Table 3. Ground- and Excited-State p*K* Values of 2–4, 6, and 7 in $CH_3CN–H_2O$ (3:2, v/v)

	ground state				excited state			
compound	pK_1	pK_2	pK_3	pK_4	pK_1*	pK_2*	pK_3*	pK_4*
2	5.66	9.33	NA	NA	5.36	9.58	NA	NA
3	5.55	9.18	NA	NA	4.76	9.20	NA	NA
4	5.04	6.14	7.21	9.09	4.85	6.39	7.55	9.12
6	4.38	7.97	NA	NA	4.63	8.15	NA	NA
7	4.32	7.02	8.81	NA	3.76	7.21	8.83	NA

dx.doi.org/10.1021/ic400449c | *Inorg. Chem.* 2013, 52, 7933–7946

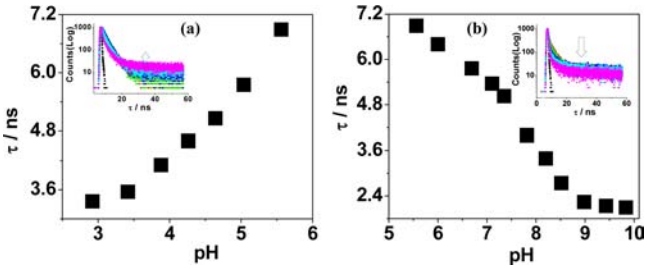

Figure 8. Change of the luminescence lifetimes of 7 with variation of the pH in acetonitrile–water (3:2, v/v). The insets show the decay profiles of 7 as a function of the pH.

in all complexes. On the other hand, upon an increase in the pH beyond 7.5, the luminescence lifetimes were found to decrease gradually. It may be mentioned that the intensity of the steady-state emission maxima of the complexes increases initially and then decreases gradually as the pH of the solution is gradually increased. It may be mentioned that the luminescence lifetimes of the complexes measured in a 3:2 (v/v) acetonitrile–water buffer solution are less compared to the lifetimes of the complexes in a pure acetonitrile medium.

The spectrophotometric data were used previously to determine the ground-state pK values of the complexes, and the luminescence data can be utilized to determine the excited-state acid dissociation constants (pK*). Because the pH ranges coincide with those observed for ground-state deprotonation of the coordinated phen-Hbzim-tpy as well as H_2pbbzim moieties of the complexes in the UV–vis titration, the above luminescence spectral changes are thus assigned to the excited-state deprotonation of the same proton, as in the ground state. Excited-state pK values could be obtained by using eq 6 from the luminescence intensity and lifetime data following the methods developed by Ireland and Wyatt.[35]

$$pK_a^* = pH + \log \tau_{acid}/\log \tau_{base} \quad (6)$$

where the pH is the inflection point of the curve of the emission intensity as a function of the pH. τ_{acid} and τ_{base} correspond to the lifetimes of the protonated and deprotonated states, respectively. The lifetime values are experimentally obtained at pH levels well above and well below the midpoint, where τ is relatively invariant with the pH. Excited-state pK* values, calculated in this way, are summarized in Table 3. The results indicate that the pK_1* values of the complexes are lower than their respective pK_1 values, while the pK_2* values are higher compared to the pK_2 values. A comparison of ground- and excited-state acid dissociation constants is useful because the relative change in the pK value provides qualitative information on the localization of charge in the MLCT states.[36−39] It is observed that the excited-state pK_1 values of the complexes are less than the ground-state pK_1 values, indicating that the excited-state electron in the complexes was mostly delocalized over the bpy/tpy moiety rather than the imidazole part of phen-Hbzim-tpy. The increased acidity in the excited state of the complexes is a consequence of Ru^{II} → ligand charge transfer principally to ligands (bpy/tpy) not involved in the proton transfer; there is a net drain of the electron density from phen-Hbzim-tpy in the excited state via electron donation to the hole of π symmetry on the ruthenium atom. The second excited-state pK_2* value is higher than the ground-state value for the same process, implying that the MLCT state is localized on phen-Hbzim-tpy (the excited state has increased negative charge and is therefore less acidic).[36−39]

CONCLUSION

In conclusion, we have successfully designed a series of redox-active and photoactive homobimetallic ruthenium(II)–ruthenium(II) and heterobimetallic ruthenium(II)–rhodium(III) complexes by using a heteroditopic phenanthroline–terpyridine bridge. The absorption spectra, redox behavior, and luminescence properties of these bimetallic complexes have been thoroughly investigated and compared with those of monometallic model compounds. Steady-state and time-resolved luminescence data at room temperature show that an efficient intramolecular electronic energy transfer from the ^{3}MLCT excited state of the $[(bpy)_2Ru^{II}(phen\text{-}Hbzim\text{-}tpy)]$-based chromophore to the ^{3}MLCT state of the tpy-containing chromophore $[(phen\text{-}Hbzim\text{-}tpy)Ru^{II}(tpy/tpy\text{-}PhCH_3/H_2pbbzim)]$ occurs in all three unsymmetrical homobimetallic complexes. On the other hand, for both heterometallic dyads, an efficient intramolecular photoinduced electron transfer from the excited-state Ru^{II} moiety to the Rh^{III}-based unit takes place. The rate constants for the energy- and electron-transfer processes have been determined by time-resolved emission spectroscopy. Another point of interest is that the emitting properties of the compounds are strongly dependent on the protonation state of the imidazole rings. In this context, the influence of the pH on the absorption, steady-state, and time-resolved emission properties of the complexes has been thoroughly investigated. This opens the possibility of the application of such compounds as proton-driven molecular switches toward the development of molecular-based electronic and photonic devices.

ASSOCIATED CONTENT

Supporting Information

ESI-MS (positive), ^{1}H and ^{1}H–^{1}H COSY NMR spectra, cyclic and square-wave voltammograms, changes in the absorption and photoluminescence spectra with variation of the pH, and changes in the excited-state lifetimes with variation of the pH of the complexes. This material is available free of charge via the Internet at http://pubs.acs.org.

AUTHOR INFORMATION

Corresponding Author

*E-mail: sbaitalik@hotmail.com.

Notes

The authors declare no competing financial interest.

ACKNOWLEDGMENTS

Financial assistance received from the Department of Science and Technology, New Delhi (Grant SR/S1/IC-33/2010), is gratefully acknowledged. Thanks are due to the DST for providing the Time-Resolved Nanosecond Spectrofluorimeter in PURSE programme at the Department of Chemistry of Jadavpur University. D.M. and S.K. thank the CSIR for their fellowship.

REFERENCES

(1) (a) Juris, A.; Balzani, V.; Barigelletti, F.; Campagna, S.; Belser, P.; von Zelewsky, A. *Coord. Chem. Rev.* **1988**, *84*, 85. (b) Balzani, V.; Juris, A.; Venturi, M.; Campagna, S.; Serroni, S. *Chem. Rev.* **1996**, *96*, 759. (c) Balzani, V.; Scandola, F. *Supramolecular Photochemistry*; Horwood:

Chichester. U.K., 1991. (d) Balzani, V.; Credi, A.; Venturi, M. *Molecular Devices and Machines*; Wiley-VCH: Weinheim, Germany, 2003. (e) Scandola, F.; Chiorboli, C.; Indelli, M. T.; Rampi, M. A. In *Electron Transfer in Chemistry*; Balzani, V., Ed.; Wiley-VCH: Weinheim, Germany, 2001; Vol. 3, p 337. (f) Welter, S.; Salluce, N.; Belser, P.; Groeneveld, M.; De Cola, L. *Coord. Chem. Rev.* **2005**, *249*, 1360.

(2) (a) Meyer, T. J. *Acc. Chem. Res.* **1989**, *22*, 163. (b) Huynh, M. H. V.; Dattelbaum, D. M.; Meyer, T. J. *Coord. Chem. Rev.* **2005**, *249*, 457.

(3) (a) Hagfeldt, A.; Grätzel, M. *Acc. Chem. Res.* **2000**, *33*, 269. (b) Sun, L.; Hammarström, L.; Akermark, B.; Styring, S. *Chem. Soc. Rev.* **2001**, *30*, 36. (c) Browne, W. R.; O'Boyle, N. M.; McGarvey, J. J.; Vos, J. G. *Chem. Soc. Rev.* **2005**, *34*, 641. (d) Balzani, V.; Clemente-Léon, M.; Credi, A.; Ferrer, B.; Venturi, M.; Flood, A. H.; Stoddart, J. F. *Proc. Natl. Acad. Sci. U.S.A.* **2006**, *103*, 1178. (e) Inagaki, A.; Akita, M. *Coord. Chem. Rev.* **2010**, *254*, 1220. (f) Chen, Z. Q.; Bian, Z. Q.; Huang, C. H. *Adv. Mater.* **2010**, *22*, 1534. (g) Baitalik, S.; Wang, X.; Schmehl, R. H. *J. Am. Chem. Soc.* **2004**, *126*, 16304. (h) Wang, X.; Guerzo, A.; Baitalik, S.; Simon, G.; Shaw, G. B.; Chen, L. X.; Schmehl, R. H. *Photosynth. Res.* **2006**, *87*, 83 and references therein.

(4) (a) Constable, E. C. *Chem. Soc. Rev.* **2004**, *33*, 246. (b) Hofmeier, H.; Schubert, U. S. *Chem. Soc. Rev.* **2004**, *33*, 373. (c) Medlycott, E. A.; Hanan, G. S. *Coord. Chem. Rev.* **2006**, *250*, 1763. (d) Medlycott, E. A.; Hanan, G. S. *Chem. Soc. Rev.* **2005**, *34*, 133. (e) Wang, X.-Y.; Del Guerzo, A.; Schmehl, R. H. *J. Photochem. Photobiol. C* **2004**, *5*, 55. (f) Baranoff, E.; Collin, J. P.; Flamigni, L.; Sauvage, J.-P. *Chem. Soc. Rev.* **2004**, *33*, 147.

(5) (a) Wong, K. M.-C.; Yam, V. W. W. *Acc. Chem. Res.* **2011**, *44*, 424. (b) Tam, A. Y. Y.; Wong, K. M. C.; Yam, V. W. W. *J. Am. Chem. Soc.* **2009**, *131*, 6253. (c) Yu, S. Y.; Sun, Q. F.; Lee, T. K. M.; Cheng, E. C. C.; Li, Y. Z.; Yam, V. W. W. *Angew. Chem., Int. Ed.* **2008**, *47*, 4551.

(6) (a) Chelucci, G.; Thummel, R. P. *Chem. Rev.* **2002**, *102*, 3129. (b) Kaveevivitchai, N.; Chitta, R.; Zong, R.; Ojaimi, M. E.; Thummel, R. P. *J. Am. Chem. Soc.* **2012**, *134*, 10721. (c) Zong, R.; Thummel, R. P. *J. Am. Chem. Soc.* **2004**, *126*, 10800.

(7) (a) Quadrelli, E. A.; Kraatz, H.-B.; Poli, R. *Inorg. Chem.* **1996**, *35*, 5154. (b) Wolf, J.; Poli, R.; Xie, J.-H.; Nichols, J.; Xi, B.; Zavalij, P.; Doyle, M. P. *Organometallics* **2008**, *27*, 5836. (c) Béthegnies, A.; Kirkina, V. A.; Filippov, O. A.; Daran, J.-C.; Belkova, N. V.; Shubina, E.; Poli, R. *Inorg. Chem.* **2011**, *50*, 12539.

(8) (a) Arm, K. J.; Williams, J. A. G. *Chem. Commun.* **2005**, 230. (b) Arm, K. J.; Williams, J. A. G. *Dalton Trans.* **2006**, 2172.

(9) (a) Harriman, A.; Hissler, M.; Khatyr, A.; Ziessel, R. *Eur. J. Inorg. Chem.* **2003**, 955. (b) Harriman, A.; Khatyr, A.; Ziessel, R. *Dalton Trans.* **2003**, 2061.

(10) (a) Constable, E. C.; Figgemeier, E.; Housecroft, C. E.; Olsson, J.; Zimmermann, Y. C. *Dalton Trans.* **2004**, 1918. (b) Figgemeier, E.; Constable, E. C.; Housecroft, C. E.; Zimmermann, Y. C. *Langmuir* **2004**, *20*, 9242.

(11) (a) Coronado, E.; Gaviña, P.; Tatay, S.; Groarke, R.; Vos, J. G. *Inorg. Chem.* **2010**, *49*, 6897. (b) Halpin, Y.; Dini, D.; Ahmed, H. M. Y.; Cassidy, L.; Browne, W. R.; Vos, J. G. *Inorg. Chem.* **2010**, *49*, 2799.

(12) (a) Bhaumik, C.; Maity, D.; Das, S.; Baitalik, S. *RSC Adv.* **2012**, *2*, 2581. (b) Bhaumik, C.; Das, S.; Maity, D.; Baitalik, S. *Dalton Trans.* **2012**, *41*, 2427. (c) Bhaumik, C.; Saha, D.; Das, S.; Baitalik, S. *Inorg. Chem.* **2011**, *50*, 12586. (d) Bhaumik, C.; Das, S.; Maity, D.; Baitalik, S. *Dalton Trans.* **2011**, *40*, 11795. (e) Bhaumik, C.; Das, S.; Saha, D.; Dutta, S.; Baitalik, S. *Inorg. Chem.* **2010**, *49*, 5049.

(13) (a) Hamelin, O.; Guillo, P.; Loiseau, F.; Boissonnet, M.-F.; Ménage, S. *Inorg. Chem.* **2011**, *50*, 7952. (b) Zheng, Z. B.; Duan, Z. M.; Zhang, J. M.; Wang, K. Z. *Sens. Actuators, B* **2012**, *169*, 312.

(14) (a) Bissell, R. A.; Córdova, E.; Kaifer, A. E.; Stoddart, J. F. *Nature* **1994**, *369*, 133. (b) Crowley, J. D.; Leigh, D. A.; Lusby, P. J.; McBurney, R. T.; Perret-Aebi, L. E.; Petzold, C.; Slawin, A. M. Z.; Symes, M. D. *J. Am. Chem. Soc.* **2007**, *129*, 15085. (c) Saha, S.; Stoddart, J. F. *Chem. Soc. Rev.* **2007**, *36*, 77.

(15) Gan, Q.; Ferrand, Y.; Bao, C.; Kauffmann, B.; Grélard, A.; Jiang, H.; Huc, I. *Science* **2011**, *331*, 1172.

(16) (a) McEvoy, J. P.; Brudvig, G. W. *Chem. Rev.* **2006**, *106*, 4455. (b) Belevich, I.; Verkhovsky, M. I.; Wilkström, M. *Nature* **2006**, *440*, 829. (c) Meyer, T. J.; Nuynh, M. H. V.; Thorp, H. H. *Angew. Chem., Int. Ed.* **2007**, *46*, 5284. (d) Ishizuka, T.; Tobita, K.; Yano, Y.; Shiota, Y.; Yoshizawa, K.; Fukuzumi, S.; Kojima, T. *J. Am. Chem. Soc.* **2011**, *133*, 18570.

(17) (a) Huynh, M. H. V.; Meyer, T. J. *Chem. Rev.* **2007**, *107*, 5004. (b) Costentin, C. *Chem. Rev.* **2008**, *108*, 2145. (c) Haga, M.; Ali, M. M.; Maegawa, H.; Nozaki, K.; Yoshimura, A.; Ohno, T. *Coord. Chem. Rev.* **1994**, *132*, 99. (d) Haga, M.; Ali, M. M.; Arakawa, R. *Angew. Chem., Int. Ed. Engl.* **1996**, *35*, 76. (e) Miyazaki, S.; Kojima, T.; Mayer, J. M.; Fukuzumi, S. *J. Am. Chem. Soc.* **2009**, *131*, 11615. (f) Manner, V. W.; Mayer, J. M. *J. Am. Chem. Soc.* **2009**, *131*, 9874. (g) Mayer, J. M. *Annu. Rev. Phys. Chem.* **2004**, *55*, 363.

(18) (a) Das, S.; Saha, D.; Mardanya, S.; Baitalik, S. *Dalton Trans.* **2012**, *41*, 12296. (b) Das, S.; Saha, D.; Karmakar, S.; Baitalik, S. *J. Phys. Chem. A* **2012**, *116*, 5216. (c) Baitalik, S.; Dutta, S.; Biswas, P.; Flörke, U.; Bothe, E.; Nag, K. *Eur. J. Inorg. Chem.* **2010**, 570.

(19) Hiort, C.; Lincoln, P.; Norden, B. *J. Am. Chem. Soc.* **1993**, *115*, 3448.

(20) Spahni, W.; Calzaferri, G. *Helv. Chim. Acta* **1984**, *67*, 450.

(21) Pott, K. T.; Usifer, D. A.; Abruna, H. D. *J. Am. Chem. Soc.* **1987**, *109*, 3961.

(22) Addison, A. W.; Rao, T. N.; Wahlgren, C. G. *J. Heterocycl. Chem.* **1983**, *20*, 1481.

(23) Sullivan, B. P.; Meyer, T. J. *Inorg. Chem.* **1978**, *17*, 3334.

(24) Perrin, D. D.; Dempsey, B. *Buffers for pH and Metal Ion Control*; Chapman and Hall: London, 1974.

(25) Kalyanasundaram, K.; Grätzel, M.; Nazeeruddin, M. K. *J. Phys. Chem.* **1992**, *96*, 5865.

(26) Frink, M. E.; Sprouse, S. D.; Goodwin, H. A.; Watts, R. J.; Ford, P. C. *Inorg. Chem.* **1988**, *27*, 1283.

(27) (a) Indelli, M. T.; Scandola, F.; Collin, J.-P.; Sauvage, J.-P.; Sour, A. *Inorg. Chem.* **1996**, *35*, 303. (b) Collin, J. P.; Lainé, P.; Launay, J. P.; Sauvage, J. P.; Sour, A. *J. Chem. Soc., Chem. Commun.* **1993**, 434.

(28) (a) Indelli, M. T.; Chiorboli, C.; Flamingi, L.; De Cola, L.; Scandola, F. *Inorg. Chem.* **2007**, *46*, 5630. (b) Indelli, M. T.; Bignozzi, C. A.; Harriman, A.; Schoonover, J. R.; Scandola, F. T. *J. Am. Chem. Soc.* **1994**, *116*, 3768.

(29) (a) Lee, J.-D.; Vrana, L. M.; Bullock, E. R.; Brewer, K. J. *Inorg. Chem.* **1998**, *37*, 3575. (b) Swaveym, S.; Brewer, K. J. *Inorg. Chem.* **2002**, *41*, 4044. (c) Zigler, D. F.; Wang, J.; Brewer, K. J. *Inorg. Chem.* **2008**, *47*, 11342. (d) Arachchige, S. M.; Brown, J. R.; Chang, E.; Jain, A.; Zigler, D. F.; Rangan, K.; Brewer, K. J. *Inorg. Chem.* **2009**, *48*, 1989. (e) Rasmussen, S. C.; Ritcher, M. M.; Yi, E.; Place, H.; Brewer, K. J. *Inorg. Chem.* **1990**, *29*, 3926.

(30) Kalyanasundaram, K. *Photochemistry of Polypyridines and Porphyrin Complexes*; Academic Press: New York, 1992.

(31) (a) Liang, Y. Y.; Baba, A. I.; Kim, W. Y.; Atherton, S. J.; Schmehl, R. H. *J. Phys. Chem.* **1996**, *100*, 18408. (b) Nozaki, K.; Ohno, T.; Haga, M. *J. Phys. Chem.* **1992**, *96*, 10880.

(32) Dexter, D. L. *J. Chem. Phys.* **1953**, *21*, 836.

(33) Förster, T. H. *Discuss. Faraday Soc.* **1996**, *27*, 7.

(34) De Cola, L.; Belser, P. *Coord. Chem. Rev.* **1998**, *177*, 301.

(35) Ireland, J. F.; Wyatt, P. A. *Adv. Phys. Org. Chem.* **1976**, *12*, 131.

(36) Montalti, M.; Wadhwa, S.; Kim, W. Y.; Kipp, R. A.; Schmehl, R. H. *Inorg. Chem.* **2000**, *39*, 76.

(37) Giordano, P. J.; Bock, C. R.; Wrighton, M. S. *J. Am. Chem. Soc.* **1978**, *100*, 6960.

(38) Hicks, C.; Ye, G.; Levi, C.; Gonzales, M.; Rutenburg, I.; Fan, J.; Helmy, R.; Kassis, A.; Gafney, H. D. *Coord. Chem. Rev.* **2001**, *211*, 207.

(39) (a) Dolberg, C. L.; Turo, C. *Inorg. Chem.* **2001**, *40*, 2484. (b) Ellerbrock, J. C.; McLoughlin, S. M.; Baba, A. I. *Inorg. Chem. Commun.* **2002**, *5*, 555. (c) Nazeeruddin, M. K.; Kalyanasundaram, K. *Inorg. Chem.* **1989**, *28*, 4251. (d) Nazeeruddin, M. K.; Müller, E.; Humphry-Baker, R.; Vlachopoulos, N.; Grätzel, M. *J. Chem. Soc., Dalton Trans.* **1997**, 4571. (e) Higgins, B.; DeGraff, B. A.; Demas, J. N. *Inorg. Chem.* **2005**, *44*, 6662. (f) Zheng, G. Y.; Wang, Y.; Rillema, D. P. *Inorg. Chem.* **1996**, *35*, 7118. (g) Wong, K. M.-C.; Tang, W.-S.; Lu, X.-X.; Zhu, N.; Yam, V. W. W. *Inorg. Chem.* **2005**, *44*, 1492.